Accelerating high-resolution NMR of half-integer quadrupolar nuclei in solids: SPAM-MQMAS and SPAM-STMAS

Akiko Sasaki, Yu Tsutsumi, Jean-Paul Amoureux

ARTICLE

Accelerating high-resolution NMR of half-integer quadrupolar nuclei in solids: SPAM-MQMAS and SPAM-STMAS

Received 00th January 20xx,
Accepted 00th January 20xx

DOI: 10.1039/x0xx00000x

Akiko Sasaki,[a] Yu Tsutsumi,[a] Jean-Paul Amoureux*[b,c,d]

In solid-state NMR, multiple-quantum MAS (MQMAS) and satellite-transition MAS (STMAS) experiments are well-established techniques to obtain high-resolution spectra of half-integer quadrupolar nuclei. In 2004 and 2005, a soft-pulse-added-mixing (SPAM) concept was introduced by Gan and Amoureux to enhance the S/N ratio of MQMAS and STMAS experiments. Despite their robustness and simplicity, SPAM approaches have not yet been widely applied. Here, we further exploit SPAM concepts for sensitivity enhancement upon acquisition of two-dimensional MQMAS and STMAS spectra and also establish a general procedure upon implementation of SPAM-MQMAS and SPAM-STMAS NMR. Its effectiveness and ease in experimental setup are demonstrated using simulations and experiments performed on I = 3/2 (^{23}Na, ^{87}Rb), 5/2 (^{27}Al, ^{85}Rb) and 9/2 (^{93}Nb) nuclei with a variety of quadrupolar coupling constants (C_Q). Compared to the conventional z-filter methods, sensitivity enhancements in between 2 and 4 are achievable with SPAM. We recommend to use SPAM with a ratio of 4:1 for the number of echoes and antiechoes to safely maximize the sensitivity and resolution simultaneously. In addition, a comparison of the experimental approaches is made in the context of SPAM-MQMAS and SPAM-STMAS NMR with respect to repetition delay and spinning frequency, aiming to discuss the precautions upon making a judicious choice of high-resolution NMR methods of half-integer quadrupolar nuclei.

1 Introduction

Quadrupolar nuclei (I > 1/2) represent more than 70% of NMR-active nuclei. Nevertheless, their use in NMR is limited owing to the presence of the quadrupole interaction which can cause a significant loss of sensitivity and resolution. In solid-state NMR of these nuclei, magic angle spinning (MAS)[1] is often employed to eliminate the first-order quadrupolar broadening and partly reduce the second-order one. For half-integer spin quadrupolar nuclei (I = 3/2, 5/2, 7/2 and 9/2), high-resolution NMR methods such as double rotation (DOR)[2] and dynamic angle spinning (DAS)[3] have been successfully implemented to obtain isotropic spectra. However, these methods require special probes with limited spinning frequencies. Multiple-quantum MAS (MQMAS)[4] and satellite-transition MAS (STMAS)[5] experiments are two-dimensional (2D) correlation experiments that allow to obtain isotropic spectra under MAS conditions. In MQMAS, a symmetrical multiple-quantum (MQ) coherence is evolved in t_1 and correlated with the central-transition (CT) coherence observed in t_2, while in STMAS, a single-quantum satellite transition (ST) is evolved in t_1 and correlated with CT in t_2. Both MQMAS and STMAS methods exploit the refocusing of the second-order quadrupolar broadening at $t_2 = Rt_1$, where the constant R depends on the spin value and the order of coherences used.[6,7] A 2D Fourier transformation (FT) of such signals leads to a 2D spectrum where each species appears as a ridge lying along the slope of R. A projection onto an axis perpendicular to R yields an isotropic spectrum free of anisotropic quadrupole interaction while a cross section along the ridge retains the anisotropically broadened MAS line-shape. Alternatively, a shearing transformation produces a 2D spectrum in which the MAS spectrum lies horizontally along the direct dimension (F_2). The isotropic spectrum can then be obtained from a projection onto the indirect dimension (F_{iso}). Although MQMAS is widely used as a routine method owing to the ease in experimental set up, its intrinsically low sensitivity due to the use of the usually 'forbidden' multiple-quantum coherences is a limiting factor in many practical applications. On the other hand, despite its high sensitivity, STMAS is more challenging to perform than MQMAS because of its technical requirements, such as stable spinning frequency and accurate magic angle setting, mandatory to eliminate the first-order quadrupole broadening.[8] MQMAS and STMAS are in fact complementary as their comparison allows to detect the presence of motions close to the various observed species.[9] For the ease of a direct comparison of all MQMAS and STMAS spectra, a unified representation has been proposed, in which an identical ppm scaling is used for F_{iso}.[10]

[a] Bruker Japan K.K., 3-9, Moriya-cho, Kanagawa-ku, Yokohama-shi, Kanagawa 221-0022, Japan.
[b] Univ. Lille, CNRS, Centrale Lille, ENSCL, Univ. Artois, UMR 8181 – UCCS – Unit of Catalysis and Chemistry of Solids, F-59000 Lille, France.
[c] Bruker Biospin, 34 rue de l'industrie, F-67166 Wissembourg, France.
[d] RIKEN RSC NMR Science and Development Division, 1-7-22 Suehiro-cho, Tsurumi-ku, Yokohama-shi, Kanagawa, 230-0045, Japan.

Electronic Supplementary Information (ESI) available. See DOI: 10.1039/x0xx00000x

In MQMAS and STMAS experiments, most often used pulse sequences are composed of three pulses: two hard pulses followed by a soft one. The initial hard pulse excites the coherence of interest (MQ or ST) and, after t_1 evolution, the second hard and the final soft pulses perform an effective conversion to observable CT coherences. Pulse sequences proposed for MQMAS and STMAS experiments to achieve absorptive line-shapes are of two categories: amplitude-modulated, which contains a z-filter,[11,12] or phase-modulated,[13,14] which is based on a full-echo acquisition. In the amplitude-modulated z-filter approach, a pair of symmetrical coherences are initially excited, evolved in t_1 and then converted to CT via a z-filtered p = 0 state selected by phase cycling. Frequency sign discrimination in t_1 is ensured by a suitable data treatment (States or TPPI). In the phase-modulated full-echo approach, on the contrary, only a single coherence pathway is selected by phase cycling. By the insertion of an appropriate interval (τ) after the second hard pulse, the echo signal is shifted in the time domain so that whole echo signals are acquired for all t_1 increments. A τ-dependent first-order phase correction gives rise to purely absorptive line-shapes. As a rule of thumb, the full-echo acquisition is often preferred for samples with long T_2' (e.g. crystalline compounds) to avoid the losses occurring during 2τ, whereas the z-filtered approach is often used for samples with short T_2' (e.g. amorphous or disordered materials). The problems of distorted line-shapes observed when using a single pathway have been discussed in detail in the case MQMAS experiments performed on a well-crystallized sample of $RbNO_3$.[15] In the following we are concerned with the amplitude-modulated approach, which is by far the most used method.

2 Soft-pulse-added-mixing (SPAM)

A large variety of sensitivity enhancement techniques (RIACT,[16] FAM,[17,18] DFS,[19] FASTER,[20] HS,[21] RAPT,[22] and QCPMG-MQMAS[23]) have been proposed and proved useful in MQMAS and/or STMAS contexts, although their optimization process may sometimes be found time-consuming owing to the presence of multiple parameters that need to be controlled. In 2004 and 2005, Gan et al.[24] and Amoureux et al.[25–27] introduced the SPAM (soft-pulse-added-mixing) concept to enhance the signal-to-noise (S/N) ratio of MQMAS and STMAS signals, and they demonstrated its simple experimental setup and successful application to ^{17}O NMR.[25–27] To illustrate the SPAM method, pulse sequences and coherence transfer pathways of triple-quantum MQMAS and DQF (double-quantum filtered) STMAS[28] experiments are shown in Fig.**1** for z-filter and SPAM approaches. All the pulse sequences mainly consist of three pulses, one for excitation (p1) and two for conversion (p2 and p3), except that the DQF-STMAS includes an additional CT-selective π-pulse (p4) immediately before the second hard pulse (p2) to remove unwanted autocorrelation peaks to simplify the spectral analysis without significant loss of sensitivity.[28] In conventional z-filter approaches (Fig.**1a**,**b**), signals from a pair of symmetrical coherence transfer pathways, echo (E) and antiecho (AE), are simultaneously selected, evolved during t_1 and converted via the z-filtered p = 0 state so that the observed signal is a combination of E and AE signals with equal amplitudes, which consequently yield a 2D absorptive line-shape. For example, p = { $\pm3 \rightarrow 0 \rightarrow -1$} is selected in z-filter MQMAS in Fig.**1a** and p = { $\pm1 \rightarrow \pm2 \rightarrow 0 \rightarrow -1$} is selected in z-filter STMAS in Fig.**1b**. In SPAM methods, on the other hand, symmetrical coherence transfer pathways are treated separately, and signals are acquired sequentially in an alternating manner. By properly setting the phase of the CT-selective p3 pulse, a constructive addition of signals from all p = (+1, 0, -1) pathways can be achieved, resulting in an effective signal accumulation. For example, as shown in Fig.**1c**-**f**, p = {+3 $\rightarrow$ (+1, 0, -1) $\rightarrow$ -1} and p = {-3 $\rightarrow$ (+1, 0, -1) $\rightarrow$ -1} are selected in SPAM-MQMAS, and p = {+1 $\rightarrow$ +2 $\rightarrow$ (+1, 0, -1) $\rightarrow$ -1} and p = {-1 $\rightarrow$ -2 $\rightarrow$ (+1, 0, -1) $\rightarrow$ -1} are selected in SPAM-STMAS, respectively. Upon consideration of Wigner rotation matrix elements, Gan indicated a possible 70% gain in signal intensity by using these (+1, 0, -1) pathways compared to that of the single p = 0 pathway.[24] Numerical simulations performed by Amoureux and co-workers revealed that the SPAM signal can be further enhanced, depending on the C_Q value, and that a maximum enhancement of ca. 2 was obtained at C_Q = 0.5-1 MHz for I = 3/2 and C_Q = 1-4 MHz for I = 5/2.[25] It should be noted that, although SPAM requires separate acquisition of E and AE signals, the total number of t_1 increments to achieve the same isotropic resolution is identical in both z-filter and SPAM experiments. This is because, in the hyper-complex (States) data treatment used in z-filter experiments, each t_1 increment is in fact recorded twice, one with sine and one with cosine modulation, to ensure frequency discrimination in the indirect dimension. Therefore, for a given experimental time, SPAM can yield a signal enhancement of up to 2 owing to the effective accumulation of signals from p = (+1, 0, -1) pathways. It should be reminded that in the conventional methods, there is a z-filter delay of a few tens of μs in between the second hard pulse (p2) and the last soft pulse (p3) to 'purge' the non-desired coherences not situated on the p = 0 state, and thus these two pulses are phase-cycled individually. With SPAM, on the contrary, these two pulses can be considered as a single composite pulse,[29] without any delay in between them, and they are thus phase-cycled globally. Since the main difference between z-filter and SPAM methods is the phase cycling that derives from the desired coherence pathways, the optimum pulse lengths are expected to be similar. This was demonstrated theoretically by Gan for p3 upon consideration of Wigner rotation matrices, and experimentally on ^{27}Al (I = 5/2) MQMAS signals of berlinite for p2 or p3.[24,26]

In addition to the implementation of SPAM into MQMAS and STMAS experiments, Amoureux et al. also introduced an additional experimental trick, namely the "truncated SPAM" for the 2D acquisition of MQMAS and STMAS signals.[25] In the truncated SPAM, either only a part or no AE signals are acquired, which we denote, "partly" and "fully"-truncated SPAM, respectively. To illustrate this concept, a time-domain representation of E and AE signals experimentally recorded on ^{27}Al (I = 5/2) of berlinite and ^{23}Na (I = 3/2) of Na_2SO_4 is shown in Fig.**2**. It should be reminded that, by definition, the signal

that moves forward in the t_2 acquisition window comes from the echo pathway, whereas the signal that moves backward and disappears from the t_2 acquisition window derives from the antiecho pathway. Therefore, for MQMAS the echo pathway during t_1 is p = -3 or +3 for I = 3/2 or ≥ 5/2, respectively. The coefficients relevant to MQMAS and STMAS experiments are summarized in Table S1 of the Supplementary Information. In a 2D time-domain representation, similar to that shown in Fig.**2**, E and AE signals move along the opposite slopes of ±1/R. For example, taking ^{27}Al (I = 5/2) MQMAS in Fig.**2a**, |R| = 19/12 and the E and AE move along the slopes of +12/19 and -12/19, respectively. As the number of t_1 increments increases, eventually, there will be a point in t_1 at which AE signals are no longer present in the t_2 acquisition window and only noise is acquired. By skipping the AE acquisition beyond this point, the total experimental time required for 2D acquisition can be largely reduced. This is schematically shown in Fig.**3** where a series of FIDs is compared between z-filter (E + AE), SPAM (E = AE), partly-truncated SPAM (0 < AE < E) and fully-truncated SPAM (AE = 0), where we designate E and AE as the number of echoes and antiechoes, respectively. In z-filter (E + AE), E and AE signals are acquired simultaneously, whereas in SPAM (E = AE), they are acquired in an alternate manner. In partly-truncated SPAM (0 < AE < E), the AE acquisition is skipped beyond an arbitrarily point and a blank dataset is inserted in place of AE signals, while in fully-truncated SPAM (AE = 0), no AE signals are acquired. With truncated SPAM approaches, a sensitivity enhancement can be simply achieved by increasing the number of scans (NS) for echo signals proportionally to the number of antiecho signals being skipped. For example, for a fixed experimental time, if no antiecho signals are recorded at all (AE = 0), then NS can be simply doubled. If the number of antiechoes is set to a quarter of the number of echoes (E:AE = 4:1), then NS can be increased by 1.6, and so on. More generally, the multiplication factor for NS is given by 2E/(E+AE). It should be noted, however, that some dispersive parts may become visible in the 2D SPAM spectra when an insufficient number of AE are recorded. This may obscure the resonances and hinder an accurate spectral analysis, especially for well-crystalized samples presenting close narrow resonances and species with small C_Q.[25] Nevertheless, successful demonstrations of SPAM experiments have been reported on two spin I = 5/2 nuclei: ^{27}Al with MQMAS of $AlPO_4$-14, or ^{17}O (enrichment < 30%) with MQMAS of $3Al_2O_3$-$48.5Na_2O$-$48.5P_2O_5$ glass,[25] and MQMAS and DQF-STMAS of $Nb_{1.91}P_{2.82}O_{12}$,[26] emphasizing the SPAM sensitivity advantage, especially in the case of distributed samples in which the absence of AE acquisition did not compromise the quality of the 2D spectra. The fully-truncated SPAM concept was also utilized in hetero-nuclear correlation (HETCOR) experiments combined with MQMAS (SPAM-MQ-HETCOR),[30] in which only an echo pathway is selected prior to population transfer via dipolar interaction (MQ-*D*-HETCOR) or J coupling (MQ-*J*-HETCOR). These high-resolution SPAM methods have been applied to ^{27}Al-^{31}P and ^{27}Al-^{29}Si through-space and through-bond HETCOR spectra and they provided a considerable sensitivity gain.[30]

Despite its robustness and simplicity, the SPAM concept has not been widely applied since its introduction and only a few number of publications exist since then.[18,29,31–33] This limited application of SPAM methods, is mainly due to three reasons: (i) solid-state NMR spectroscopists rarely use the echo-antiecho method, (ii) the data treatment of the truncated SPAM methods was not easy to do before, and (iii) no simple rule for the best E:AE ratio was proposed. However, (i) this complexity of the data treatment is now completely overcome with the new NMR consoles, (ii) we provide in this article a simple rule for the E:AE ratio, and (iii) very simple and robust SPAM sequences are presently available (see Supplementary Information). Here, we further exploit the SPAM approach to accelerate the acquisition of MQMAS and STMAS spectra with respect to sensitivity. Its effectiveness and ease in experimental setup are demonstrated using both simulations and experiments performed on I = 3/2 (^{23}Na, ^{87}Rb), 5/2 (^{27}Al, ^{85}Rb) and 9/2 (^{93}Nb) nuclei with a wide range of C_Q values. It will be shown that sensitivity enhancements of up to 4 can be attained by SPAM-MQMAS and SPAM-STMAS without additional time-consuming pulse optimization. Recent developments of high-field (B_0) spectrometers and fast MAS probes have potential to facilitate the solid-state NMR investigations of half-integer quadrupolar nuclei. In the context of SPAM, we also present a comparison of several experimental approaches with respect to repetition delay (RD) and spinning frequency (ν_R), discussing the precautions upon making a judicious choice of high-resolution NMR methods (MQMAS versus STMAS) for half-integer quadrupolar nuclei in solids.

3 Methods

All experiments were performed using a Bruker Avance NEO spectrometer with a B_0 = 14.1 T wide-bore magnet at a Larmor frequency of 158.75 (^{23}Na), 156.38 (^{27}Al), 196.37 (^{87}Rb), 57.94 (^{85}Rb) and 146.89 (^{93}Nb) MHz, equipped with HX MAS probes using either ∅ = 3.2 mm rotors at ν_R = 20-22 kHz or ∅ = 1.3 mm at ν_R = 20 and 62.5 kHz. For hard pulses, maximum rf field strengths of ν_1 = 120 (^{87}Rb), 95 (^{23}Na), 90 (^{27}Al), 35 (^{85}Rb) kHz were attained with ∅ = 3.2 mm, and ν_1 = 160 (^{87}Rb), 128 (^{93}Nb) kHz with ∅ = 1.3 mm. A range of ν_1 = 5-20 kHz was used for CT-selective soft pulses. Powder samples (Na_2SO_4, NaH_2PO_4, sodium citrate dihydrate, $AlPO_4$-14, Berlinite, γ-Al_2O_3, $RbNO_3$, Rb_2SO_4, $NaVO_3$, $CS_4Nb_{11}O_{30}$, and $Nb_3(NbO)_2(PO_4)_7$) were packed as purchased or as synthesized. All MQMAS experiments were performed using the triple-quantum versions described in Fig.**1a**,**c** and all STMAS ones with the DQF (double-quantum filtered) versions described in Fig.**1b**,**d**. The coefficients of MQMAS and STMAS experiments and quadrupolar parameters of selected compounds are provided in Tables S1 and S2, respectively. Prior to any 2D signal acquisition, for each sample all pulse lengths were experimentally optimized using a 1D version that corresponds to either the first row or the first echo of the 2D acquisition, for z-filter or SPAM experiments, respectively. Chemical shift

scales, shown in ppm, were referenced using the sample of interest itself as a secondary reference, and MQMAS and STMAS spectra were referenced after shearing transformation according to the unified representation.[10] Prior to any STMAS investigations, accurate adjustment of the spinning axis to the magic angle was performed using a DQF version of the split-t_1 shifted-echo pulse sequence on the sample of interest itself.[34] Further experimental details are given in the figure captions.

We used the TS4.0.6 version of Topspin software. It must be noted that with previous versions, in the case of for I = 3/2 nuclei the minimum number of AE that can be acquired with SPAM is not 0, but 1.

All simulations were performed using the SIMPSON density matrix simulation program.[35] The variable input parameters were the nucleus of interest, spinning frequency (ν_R), rf field strength (ν_1), and the quadrupolar coupling constant (C_Q). The quadrupole interaction, with $\eta_Q = 0$, was taken into account up to the second-order, without scalar or dipolar coupling. Input pulse programs and coherence selections were chosen to emulate the real MQMAS and STMAS sequences shown in Fig.**1** without any delay, except for the rotor-synchronized STMAS experiments ($t_{1min} = T_R$ - p1/2 - p4 - p2/2). All pulses were applied on the gravity center of the line-shape using ν_1 = 90-160 kHz for hard pulses and ν_1 = 5-20 kHz for CT-selective soft pulses. Input parameters intrinsic to powder averaging under MAS conditions (crystal file, number of γ-angles and maximum time step (Δt) over which the Hamiltonian is considered time independent) were tested for convergence, and a combination of ZCW20 $\times$ 10 γ-angles with Δt = 0.1 μs was sufficient to produce a contour plot of signal intensity versus pulse lengths for the given range of C_Q used in the following investigations. Since the imaginary part of the signal was found to be minor, only the real part of the signal is plotted as the signal intensity. Further computational details are given in the figure captions.

4 Results and discussion

4-1 Pulse length optimization

As previously discussed by Gan[24] and Amoureux,[26] the optimum pulse lengths for SPAM are expected to be close to those of z-filter. This has been verified using simulations. Fig.**4** shows a series of plots of calculated MQMAS and STMAS signal intensities with respect to each pulse length for a large range of C_Q values for ^{27}Al (I = 5/2) and ^{23}Na (I = 3/2) nuclei. Only the signal intensity of the echo pathway has been considered since it gives rise to the overall signal intensity, while the antiecho signal mainly contributes to cancel the residual dispersive part of the echo signals.

Upon comparison of contour plots between z-filter and SPAM, it can be observed that the optimum pulse lengths are identical in both MQMAS and STMAS approaches. For example, for ^{27}Al with C_Q = 4 MHz, the optimum MQMAS pulse lengths for z-filter and SPAM are {p1, p2, p3} = {4.0, 1.4, 16.7} μs, and similarly {p1, p2, p3, p4} = {1.8, 1.1, 16.7, 33.4} μs for both z-filter and SPAM-STMAS approaches.

Since the optimum pulse lengths are identical with z-filter and SPAM, no additional experimental time is required for further optimization upon implementation of SPAM experiments. This makes SPAM a simple, efficient and user-friendly approach compared to other sensitivity enhancement techniques that might involve complicated and time-consuming parameter optimization procedure.

4-2 Sensitivity enhancement and reduction in experimental time

Despite their robustness and simplicity, SPAM methods have not been widely used since their introduction and not many examples are available in the literature to demonstrate the effectiveness of SPAM as a sensitivity enhancement technique for MQMAS and STMAS acquisition. In the following subsections, we present a selected series of comparison of MQMAS and STMAS spectra of inorganic crystalline powder samples with various C_Q values for I = 3/2 (^{23}Na, ^{87}Rb) or 5/2 (^{27}Al, ^{85}Rb).

We show that, for a given experimental time, a signal enhancement of 2 to 4 is easily achieved by SPAM compared to z-filter. In addition, although SPAM was originally developed for sensitivity gains of MQMAS and STMAS signals, it can readily be used for reduction of the experimental time to obtain an identical isotropic spectrum. In the following, three sets of MQMAS or STMAS experiments were compared: z-filter, SPAM (E = AE), and truncated SPAM ($0 \leq AE < E$) in which the AE acquisition is partly or fully skipped. An identical combination of optimum pulse lengths was used in z-filter and SPAM, as anticipated from the simulations and confirmed experimentally.

4-2-1 Sensitivity enhancement

Figs.**5a**,**b** show a comparison of isotropic projections of ^{27}Al ($AlPO_4$-14) MQMAS and ^{87}Rb (Rb_2SO_4) STMAS spectra recorded using z-filter and SPAM approaches. The experimental time (T_{exp}), repetition delay (RD), and total number of t_1 increments (Nt1) were fixed, while the number of scans (NS) was the same in z-filter and SPAM (E = AE) but doubled in fully truncated SPAM (AE = 0 or 1) to amount to the same T_{exp}. Compared to z-filter, the signal intensity of SPAM (E = AE) is twice as large, as anticipated by the previous numerical simulations[25] and our simulated contour plots in Fig.**4**. This signal enhancement originates from the constructive addition of (+1, 0, -1) coherences intrinsic to the SPAM concept. With the fully truncated SPAM (AE = 0), a signal enhancement of 4 can be observed with respect to z-filter. This gain can be decomposed as 2 $\times$ 2, where the first factor of 2 comes from the constructive addition of (+1, 0, -1) coherences intrinsic to SPAM and the second is related to the doubling of NS to compensate for the time saved by skipping the AE acquisition. For example, in the case of ^{27}Al MQMAS of $AlPO_4$-14 in Fig.**5a**, 24 scans were accumulated for each of 256 t_1 increments in z-filter, 24 scans for each of 128 E and 128 AE acquisition in SPAM (E = AE), and 48 scans for each of 128 E acquisition in fully-truncated SPAM (AE = 0). It can be concluded that, for a

given T_{exp}, a signal enhancement of 2 is attainable by SPAM (E = AE) and of 4 by fully truncated SPAM (AE = 0).

4-2-2 Reduction in experimental time

Although SPAM was originally developed to increase the intensity of MQMAS and STMAS signals, it can also be used to reduce T_{exp} to obtain an identical isotropic spectrum. Figs.**5c**,**d** show the isotropic projections of ^{27}Al MQMAS of berlinite or ^{23}Na STMAS of NaH_2PO_4, and the experimental times to achieve such identical isotropic resolutions. With respect to z-filter, SPAM (E = AE) and fully truncated SPAM (AE = 0) can be twice and four times faster, respectively. For example, in the ^{27}Al MQMAS case of berlinite (Fig.**5c**), to obtain the same isotropic projections, recording the z-filter took 4 hrs (24 scans × 200 t_1 increments), SPAM (E = AE) 2 hrs (12 scans × (100 E + 100 AE)), and truncated SPAM 1.2 hrs (12 scans × (100 E + 20 AE)). This considerable time-saving advantage of SPAM, as well as the associated sensitivity gain, are particularly useful when the isotropic signal acquisition via MQMAS or STMAS is combined with other experiments such as hetero-nuclear correlation experiments.[30]

4-3 Analysis of SPAM 2D spectra

So far, only the isotropic 1D projections were used to demonstrate the advantages of SPAM over z-filter. However, as the integrated surface of the dispersion is always zero, these 1D isotropic projections are immune to any dispersive signal. This is not the case of the SPAM 2D spectra. The E signal is directly related to the intensities of the 2D line-shapes, while the AE signal cancels the dispersive parts of the resonances to achieve absorptive line-shapes.[25] This implies that, when an insufficient number of AE signals is acquired, some dispersive parts may become apparent in the 2D SPAM spectra, possibly hindering an accurate spectral analysis. However, it has been shown experimentally that only a small number of AE is required to minimize the dispersion of distributed samples such as glasses,[26] while a significant number of AE may be necessary for crystalline materials.[25,29] This presence of dispersion is systematically illustrated in Fig.**6** using ^{85}Rb MQMAS and STMAS spectra of $RbNO_3$. In z-filter STMAS (Fig.**6a**), three Rb sites, with Rb1 and Rb3 overlapping, are clearly present, whereas in z-filter MQMAS (Fig.**6d**), the Rb2 site with the largest C_Q is barely visible. In the isotropic projection of these spectra, the signal intensity of STMAS is approximately 5 times higher than that of MQMAS. In SPAM (E = AE) spectra (Fig.**6b**,**e**), the signal intensity is doubled with respect to that of z-filter, as expected. In fully truncated SPAM spectra (Fig.**6c**,**f**), the signal intensity is scaled up by a factor of 4 as NS was doubled. In the fully truncated SPAM-STMAS spectrum (Fig.**6c**), however, the dispersive tails are significantly visible above the noise due to the lack of cancellation by AE signal. This is not the case with the fully truncated SPAM-MQMAS spectrum (Fig.**6f**), in which the dispersive tails are just above the noise level. This is related to the fact the dispersion is proportional to the signal intensity and that STMAS exhibits a ca. five times higher signal intensity than MQMAS for this compound.

A question that arises here is, "is it possible to find a ratio of the number of echo and antiecho (E:AE), in between 1:1 and 1:0, which simultaneously minimizes the dispersion and maximizes the intensity even for species with small C_Q in well-crystallized samples?" In order to answer this question, a set of SPAM (E = AE) spectra were recorded for well-crystallized samples containing nuclei with I = 3/2 (^{23}Na, ^{87}Rb) and 5/2 (^{27}Al, ^{85}Rb) with various C_Q values. Starting from the experimental SPAM (E = AE) dataset, a series of truncated SPAM ensembles with arbitrary E:AE ratios were then created by zero-filling the data points that correspond to the skipped AE signals. This processing is schematically illustrated in Fig.**S1**, using an experimental SPAM dataset with E = AE = 50 as an example. The series of time-domain SPAM datasets with arbitrary E:AE ratios were then Fourier-transformed and the resulting 2D spectra were analyzed qualitatively (Fig.**7**), by the examination of the spectral appearance, and quantitatively (Fig.**8**), by calculating the ratio between negative and positive integrals over an arbitrary area of 2D spectra.

Fig.**7** shows two examples of qualitative examination of the spectral appearance of a series of 2D SPAM spectra of well-crystallized samples with arbitrary E:AE ratios. In ^{27}Al SPAM-MQMAS spectra of $AlPO_4$-14, the large C_Q sites (Al2 and Al3) are already absorptive even with AE = 0, while the small and moderate C_Q sites (Al1 and Al4) give rise to dispersive tails. With AE = 16 (E:AE = 8:1), the moderate C_Q site (Al4) becomes absorptive and eventually all sites are absorptive with AE = 32 (E:AE = 4:1). Similarly, in ^{87}Rb SPAM-STMAS spectra of Rb_2SO_4, the larger C_Q site (Rb2) is already absorptive even with AE = 1, and as the number of AE increases, both sites become absorptive with AE = 19 (E:AE = 4:1). From this spectral appearance of well-crystallized samples, one deduces that fully-truncated SPAM can be used for large C_Q sites. On the contrary, for small C_Q sites, truncated SPAM with E:AE ≈ 4:1 is better to minimize the dispersion and maximize the signal intensity simultaneously.

As for the quantitative analysis, Fig.**8** summarizes the ratio of negative to positive integrals (–/+) of the resonances plotted versus the ratio of the number of AE to that of E (AE/E) for various C_Q values. The integrals were calculated over an arbitrary area of 2D spectra, and they are assumed proportional to dispersion and signal intensity, respectively. The convergence was tested for I = 5/2 (^{27}Al and ^{85}Rb) and I = 3/2 (^{87}Rb and ^{23}Na). It can be seen that the ratio of negative to positive integrals decreases as the ratio AE/E increases from zero and it is minimum at E:AE = 4:1. There is no change in this ratio (–/+) when AE > E/4, i.e. no further minimization of dispersion. This is in good agreement with the qualitative analysis made on the examination of spectral appearance of 2D SPAM spectra (Fig.**7**).

Based on the qualitative and quantitative analyses made in this section, the use of truncated SPAM with E:AE = 4:1 is recommended for small C_Q sites with well-crystallized samples, whereas that of fully truncated SPAM seems to be possible for large C_Q sites. This potential use of AE = 0 may look surprising

because of the dispersive components that exist in the 2D line-shapes. However, it must be first reminded that for each crystallite, the dispersive component corresponds to a 2D signal with positive and negative parts. This means that in the case of a powder sample, these dispersive components cancel each other's in the central part of broad 2D resonances. This cancellation process cannot fully occur in the case of narrow resonances or on the external parts of broad resonances. However, it must be remembered that skipping all AE allows doubling the signal with respect to the case "E = AE". Most of the time the spectrometer time is limited, and it may be interesting to divide by 2 a long acquisition time, even if this introduces a small amount of dispersion. It is important to remind that complete MQMAS and STMAS 2D line-shape simulations are very difficult to perform. Indeed, to be accurate these simulations should have to take care of numerous parameters such as: (i) distribution of surroundings, (ii) rf-field inhomogeneity, (iii) pulse transients, (iv) Q of the probe, and (v) fluctuations of spinning-speed and magic-angle in the case of STMAS!

To demonstrate the small distortions afforded with a limited number of AE in the case of a moderately distributed sample, we have recorded the ^{27}Al SPAM-MQMAS 2D spectrum of γ-alumina, with AE = E = 25, and we have treated the data a posteriori with a decreasing number of AE. The results, shown in Fig.**9**, demonstrate that no spectral distortion is observed when E:AE $\leq$ 6:1.

As a conclusion, we recommend using the ratio E:AE = 4:1, which simultaneously minimizes the dispersion and maximizes the intensity in all types of samples (well-crystalized or not) and C_Q values (small or large).

4-4 Detection of minor signals: ^{23}Na (I = 3/2: $NaVO_3$)

In the previous section, we demonstrated the sensitivity advantage of truncated SPAM (E:AE = 4:1). We should note, however, that this advantage is only effective when a sufficient number of echoes is recorded, i.e. the echo signals decayed completely in t_1, as for all other MQMAS and STMAS methods.

A question may arise: what is the best sequence for the detection of minor quadrupolar signals under high resolution? This problem is analyzed in Fig.**10** showing ^{23}Na spectra of commercial $NaVO_3$. This sample is known to consist of α- and β-$NaVO_3$ polymorphs,[36] and from the MAS line-shape shown in Fig.**10a**, our sample seems to contain mostly β-$NaVO_3$ and a tiny amount of α-$NaVO_3$, with {C_Q (MHz), η_Q, δ_{CS} (ppm)} = {1.42, 0.27, -10.3} for β-$NaVO_3$ and {Na1: 1.50, 0.58, -15.6} plus {Na2: 0.765, 0.06, -4.8} for α-$NaVO_3$. Figs.**10b**-**d** show the ^{23}Na z-filter, SPAM (E = AE = 96) and truncated SPAM (E:AE = 96:24 = 4:1) STMAS 2D spectra of $NaVO_3$, with the corresponding isotropic projections below, expanded for minor resonances in Figs.**10e**-**g**. It can be seen that the isotropic signal intensities of minor signals increase from z-filter to SPAM (E:AE = 4:1) by a factor of ca. 4, as expected. However, a significant baseline distortion is introduced in the isotropic projection. This distortion, is intrinsic to STMAS due to the rotor-synchronized non-zero evolution time: $t_{1min} = T_R$ - p1/2 - p4 - p2/2. It is also at the origin of the negative green parts in the 2D spectra of Fig.**10c** and **d** and being proportional to the signal is hence doubled in Fig.**10d** compared to Fig.**10c**. These dispersive parts may be cancelled afterward by using a linear prediction. However, one also observes that the detection of these minor species remains easy on the isotropic projection (Fig.**10g**). We should note that the use of MQMAS to detect these minor signals is very inefficient as its signal intensity was found four times lower than that of STMAS for this sample.

4-5 Comparison of experimental approaches

The recent development of high-field spectrometers and fast MAS techniques has made solid-state NMR investigations of half-integer quadrupolar nuclei more and more accessible, owing largely to the intrinsic increase in sensitivity at high B_0 fields and a possible resolution enhancement by the narrowing effect of MAS line-width under fast MAS conditions. When a given sample of interest is suspected to possess overlapping multiple sites with possibly distributions of chemical shifts or quadrupolar couplings, it has become routine for solid-state NMR users to record high-resolution spectra.

For a finite spectrometer time, NMR spectroscopists are often required to make a strategic decision on hardware, methods and parameters to be used. While STMAS requires an accurate orientation for the rotor axis and a stable spinning speed to cancel the 1st-order quadrupole interaction, the intrinsic insensitivity of MQMAS may demand a large number of scans (NS) and hence a long experimental time (T_{exp}). Fast MAS conditions may narrow the CT MAS linewidth of nuclei subject to large quadrupolar interactions and hence may increase the resolution between overlapping sites. However, the sample volume is then inevitably decreased, and the rotor-synchronized MQMAS and STMAS acquisitions may require a larger number Nt_1 of increments and hence a longer T_{exp}. Furthermore, the choice of the repetition delay (RD) may affect the relative intensities if multiple sites with different T_1 are present. For a given spectrometer time, therefore, an interplay between the choice of (i) method, (ii) spinning frequency, (iii) repetition delay, (iv) number of scans and (v) number of t_1 increments, controls the quality of high-resolution spectra of half-integer quadrupolar nuclei.

In the following, a comparison of experimental approaches is made in the context of ^{23}Na and ^{87}Rb (I = 3/2) SPAM-MQMAS and SPAM-STMAS experiments with respect to repetition delay and spinning frequency, aiming to discuss the precautions upon making a judicious choice of high-resolution NMR methods of half-integer quadrupolar nuclei. Also, ^{93}Nb (I = 9/2) NMR of previously studied compounds is revisited to demonstrate the applicability of MQMAS and STMAS experiments to this nucleus in the context of SPAM approaches.

4-5-1 Repetition delay: ^{23}Na (I = 3/2: sodium citrate dihydrate)

So far, only the absolute signal intensity of the indirect isotropic projection was considered to demonstrate the SPAM enhancement, on assumption that the t_1 noise is insignificant compared to the signal intensity. In the direct dimension, however, the thermal noise makes a significant contribution. A comparison of the theoretically expected maximum of S/N

ratios of z-filter and SPAM approaches is summarized in Table 1. With SPAM (E:AE = 1:1), a maximum signal gain of 2 is expected while the noise increases by a factor of $\sqrt{2}$ as the E and AE signals are acquired separately and then combined upon processing. This gives rise to a gain of S/N of 1.4 with SPAM (E:AE = 1:1). With SPAM (E:AE = 4:1), NS is scaled up by a factor of 1.6 = 2E/(E+AE) and thus the maximum signal gain is 2 $\times$ 1.6 = 3.2, resulting in a gain of S/N of 2.3 = 3.2/$\sqrt{2}$.
These expected values have been experimentally verified in the following with ^{23}Na MQMAS and STMAS investigations.

In Fig.**S2**, we show a signal recovery profile of ^{23}Na MAS spectra of sodium citrate dehydrate versus the repetition delay (RD). From this profile $T_1 \approx 1.5$ s, and we expect that 50 and 97 % recoveries are ensured with RD = 0.5 and 5 s, respectively. For a given spectrometer time, we have set up ^{23}Na MQMAS and STMAS experiments with RD = 0.5 and 5 s, as summarized in Table 2. It should be remembered that the number of t_1 increments (Nt_1) to achieve the same isotropic resolution is twice in STMAS that in MQMAS (Table S1).[10] Consequently, the numbers Nt_1 of increments required to achieve the same isotropic resolution are also in the ratio of 2. In the case of sodium citrate dehydrate, Nt_1 = 96 and 192 were chosen, and the number of scans was then adjusted in the unit of minimum phase cycling (24 for MQMAS, 12 for SPAM-MQMAS, 32 for STMAS and 16 for SPAM-STMAS) so that $T_{exp} \approx$ 9 hours.

Fig.**11** compares the isotropic MQMAS and STMAS projections of ^{23}Na z-filter and SPAM (E:AE = 4:1) spectra recorded according to the experimental set up in Table 2. We should note that the relative intensities of isotropic peaks are modified when RD changes (compare Figs.**11b** and **d** or **f** and **h**), and it is highly likely that T_1(Na2) < T_1(Na1, Na3). It should be reminded that MQMAS is 3-5 times less sensitive than STMAS. This results in an apparently low intensity of Na1 in MQMAS compared to STMAS, most apparent when comparing Figs.**11b** and **f**. Nonetheless, the signal gain by SPAM over z-filter was observed to be in the range of 2.8-3.3, which is in good agreement to the theoretically expected value of ca. 3.2 for SPAM (E:AE = 4:1) in Table 1. Similarly, the S/N gain by SPAM lies in the range of 1.6-2.7 (calculated from the last three lines of Table 2), which corresponds to the theoretically expected value of ca. 2.3 in Table 1. For a given experimental time, SPAM-STMAS (E:AE = 4:1) is likely to be the method of choice to achieve an optimum sensitivity, i.e. the highest S/N in Table 2. Moreover, upon comparison of the integrated intensities of the isotropic projections of Figs.**11b**,**d**,**f**,**h**, a long relaxation value (RD = 5 s $\approx 3T_1$ here) looks to provide better-quantified isotropic spectra with integrated ratios close to 1:1:1.

4-5-2 Spinning frequency: ^{87}Rb (I = 3/2: Rb_2SO_4)

Recent developments of fast MAS techniques have undoubtedly broadened the scope of solid-state NMR. In the context of MQMAS and STMAS, increasing the spinning speed enhances the resolution by zeroing the CSA and dipolar interactions, and by narrowing the MAS line-width in case of very large C_Q values, which facilitate the signal acquisition. It also increases the isotropic spectral widths of rotor-synchronized experiments, SW_{iso}, which are proportional to this spinning speed, thus limiting the folding of the resonances, which greatly eases the subsequent spectral analysis.

These effects are demonstrated in Fig.**12** using ^{87}Rb z-filter MQMAS and STMAS spectra of Rb_2SO_4 recorded with ν_R = 20 and 62.5 kHz using a 1.3 mm rotor. It can be seen that SW_{iso} is doubled in STMAS with respect to MQMAS (as mentioned in the previous section) and that it increases proportionally to ν_R. It should be remembered, however, that the number Nt_1 of increments to achieve the same isotropic resolution increases proportionally to SW_{iso}, hence leading to longer experimental times. For example, for MQMAS in Fig.**12a**,**c**, Nt_1 = 50 and 160 increments were used at ν_R = 20 and 62.5 kHz, respectively. Nevertheless, the larger SW_{iso} reduces the risk of signal aliasing or spectral crowding and alleviates the subsequent spectral analysis. Another advantage of fast MAS techniques is the fact that they are associated to small rotor diameters that can deliver very high rf-fields, which are highly recommended for the p1 and p3 hard pulses, and are difficult to access for low-γ nuclei.[37] Consequently, fast MAS conditions offer a possibility of widening the range of C_Q that can be investigated by high-resolution NMR methods. Fig.**13** shows a series of ^{87}Rb signal intensities simulated with ν_R = 20 and 62.5 kHz for a range of C_Q. It has been known that MQMAS efficiency decreases when ν_R increases,[37] as shown in our simulations (Fig.**13a**,**b**) and experiments (Fig.**12a**,**c**). On the other hand, STMAS requires rotor-synchronized delays to refocus the large first-order broadening. The minimum evolution time is not zero but $t_{1min} = T_R$ - p1/2 - p4 - p2/2. The 2D signal intensities are determined by the signal at t_{1min} and they are thus attenuated by the losses that occur during this minimum delay due to irreversible processes and second-order quadrupolar dephasings that are not refocused by MAS. Under fast MAS conditions, however, these losses are minimized and hence the STMAS efficiency increases, especially for large C_Q values. This is confirmed by our simulations (Fig.**13c**,**d**) and experiments (Fig.**12b**,**d**) in which the intensities of isotropic peaks are 3-4 times larger at ν_R = 62.5 compared to 20 kHz.

Fig.**14** shows a series of isotropic projections of ^{87}Rb MQMAS and STMAS spectra of Rb_2SO_4 recorded with various SPAM approaches. As expected from simulations (Fig.**13**), the optimum pulse lengths are identical with z-filter and SPAM, irrespective of ν_R. With STMAS, the expected signal enhancements of 2 ($\approx$ 1.9) and 4 ($\approx$ 3.8) were observed for SPAM (E = AE) and SPAM (E:AE = 4:1), respectively. With MQMAS, slightly larger enhancements of 2.7-2.8 and 5.5-5.6 were observed, but these gains are difficult to accurately determine due to the poor S/N of z-filter signals. Considering that the STMAS sensitivity is approximately 5 times larger than that of MQMAS for this sample, the use of SPAM-STMAS under fast MAS conditions is a promising approach to expand the range of C_Q that can be investigated by high-resolution NMR.

4-5-3 Application to ^{93}Nb (I = 9/2)

We demonstrated in Fig.**2**, that the slopes of $\pm$1/R along which the E and AE signals move in time depend on the spin

value and the nature of the coherences used (MQMAS or STMAS). Taking ^{27}Al (I = 5/2) in Fig.2a as an example, the MQMAS signals move along the slopes of ±0.632 (±12/19), while the STMAS slopes are equal to ±3.429 (±24/7). Consequently, the AE signal disappears from the t_2 acquisition window much faster in MQMAS than in STMAS. This effect is still more pronounced for MQMAS of I = 9/2 nuclei, for which the slopes are very small and equal to ±0.396 (Table S1) and thus very few AE may be visible in t_2 acquisition window.

^{93}Nb (I = 9/2) nuclei have 100 % natural abundance and a relatively high gyromagnetic ratio. However, they exhibit a large chemical shift range (≈ 4000 ppm) and their solid-state NMR spectra are often severely broadened due to large quadrupolar coupling. Both aspects inhibit the extraction of useful information concerning ^{93}Nb nuclei. Following the development of high-field spectrometers and fast MAS probes, ^{93}Nb solid-state NMR spectra recorded at 21.1 T[38] and ν_R = 60 kHz have been reported,[39] and ^{93}Nb solid-state NMR has indeed become more accessible as a reliable tool for material characterization.[39,40] Although numerous static and MAS studies of Nb-containing compounds exist, only a limited number of high-resolution MQMAS and STMAS spectra have been reported.[14,31,38,41–45] Combined with the recent acceleration in first-principles calculations of ^{93}Nb NMR parameters,[39,44–49] high-resolution NMR methods have great potential to facilitate the use of ^{93}Nb solid-state NMR in material investigations.

Fig.15 shows a series of simulated ^{93}Nb signal intensity at 14.1 T with ν_R = 20 and 62.5 kHz for a range of C_Q. These results confirm that, as discussed in the former sections, (i) the optimum pulse lengths are identical between z-filter and SPAM, and (ii) that when the spinning speed increases, the MQMAS efficiency decreases while that of STMAS increases, especially for large C_Q values.

^{93}Nb spectra of $Nb_3(NbO)_2(PO_4)_7$ and $Cs_4Nb_{11}O_{30}$ recorded at 18.8 T and 20 kHz MAS have been reported.[31] Fig.16 shows a series of isotropic slices of MQMAS and STMAS spectra of $Nb_3(NbO)_2(PO_4)_7$ with ν_R = 20 or 62.5 kHz. Under these conditions, the STMAS intensity is roughly 3.5 times higher than MQMAS. Although we observed the expected SPAM enhancement, ν_R = 20 kHz was not fast enough and a partial overlap of the center-band and the first spinning sidebands of the CT was observed in the MAS spectra. Also, the isotropic MQMAS spectra at ν_R = 20 kHz (Fig.16a) are severely aliased, demonstrating the superiority of faster spinning with larger spectral width. Although the previous study suggested C_Q = 30 MHz,[31] we suspect the presence of peaks with much smaller C_Q in our sample, which are probably the cause of sinc wiggles visible in the MQMAS spectra at 62.5 kHz spinning (Fig.16b). The signal truncation is less pronounced in the STMAS spectra (Fig.16d) as the signal intensity of the main peak with large C_Q is much higher than that of MQMAS.

Fig.S3 shows a similar series of isotropic slices of MQMAS and STMAS spectra of $Cs_4Nb_{11}O_{30}$ recorded with various SPAM approaches. Under these conditions, the STMAS intensity was found approximately 6.5 times higher than that of MQMAS for this sample with C_Q = 16 MHz.[31]

Overall, for ^{93}Nb isotopes we recommend the use of STMAS at ν_R = 62.5 kHz for optimum sensitivity and resolution.

5 Conclusions

The main purpose of this publication is to describe the successful implementation of SPAM high-resolution experiments for half-integer quadrupolar nuclei. This has been done for spin-3/2, 5/2 and 9/2 nuclei in inorganic compounds with known NMR parameters. We have shown that a signal gain of ca. 4 and a gain in S/N of ca. 2.3 can be expected with the same simple setting than with z-filter. We have shown that SPAM-STMAS provides a much larger signal than the mostly used z-filter MQMAS. It has been shown recently that with an adapted Bruker MAS iProbe and a modern speed controller, the technical difficulties usually related to STMAS are fully controlled, which means than now high-resolution of half-integer quadrupolar nuclei can be obtained, even with insensitive compounds. The sensitivity advantage of SPAM will be particularly helpful for signal acquisition of nuclei or samples with intrinsically low S/N such as low-γ, low natural abundance and/or large C_Q. We expect that SPAM-MQMAS and SPAM-STMAS experiments will be a promising approach for further applications, in which signal acquisitions using conventional pulse sequences have been unsuccessful, or for more sophisticated experiments such as efficient isotropic signal acquisition in high-resolution hetero-nuclear correlation experiments. We believe that these results will be presented elsewhere in the foreseeable future.

Conflicts of interest

There are no conflicts to declare.

Acknowledgements

The authors would like to thank Dr. Hideaki Kimura (Bruker Japan K.K.) and Dr. Sebastian Wegner (Bruker GmbH) for their help with implementation of SPAM experiments on TopSpin, and Dr. Julien Trébosc (University of Lille) for his kind advice on performing SIMPSON simulations.

References

1 E. R. Andrew, A. Bradbury and R. G. Eades, *Nature*, 1958, 182, 1659.
2 A. Samoson, E. Lippmaa and A. Pines, *Mol. Phys.*, 1988, **65**, 1013–1018.
3 A. Llor and J. Virlet, *Chem. Phys. Lett.*, 1988, **152**, 248–253.
4 L. Frydman and J. S. Harwood, *J. Am. Chem. Soc.*, 1995, **117**, 5367–5368.
5 Z. Gan, *J. Am. Chem. Soc.*, 2000, **122**, 3242–3243.
6 J. P. Amoureux, *Solid State Nucl. Magn. Reson.*, 1993, **2**, 83–88.
7 J. P. Amoureux and C. Fernandez, *Solid State Nucl. Magn. Reson.*, 1998, **10**, 211–223.
8 C. Huguenard, F. Taulelle, B. Knott and Z. Gan, *J. Magn. Reson.*,

2002, **156**, 131–137.
9 S. E. Ashbrook, S. Antonijevic, A. J. Berry and S. Wimperis, *Chem. Phys. Lett.*, 2002, **364**, 634–642.
10 J. P. Amoureux, C. Huguenard, F. Engelke and F. Taulelle, *Chem. Phys. Lett.*, 2002, **356**, 497–504.
11 J. P. Amoureux, C. Fernandez and S. Steuernagel, *J. Magn. Reson. A*, 1996, **123**, 116–118.
12 Z. Gan, *J. Chem. Phys.*, 2001, **114**, 10845–10853.
13 S. P. Brown and S. Wimperis, *J. Magn. Reson.*, 1997, **124**, 279–285.
14 S. E. Ashbrook and S. Wimperis, *J. Magn. Reson.*, 2002, **156**, 269–281.
15 T. Vosegaard, P. Florian, P. J. Grandinetti and D. Massiot, *J. Magn. Reson.*, 2000, **143**, 217–222.
16 G. Wu, D. Rovnyak and R. G. Griffin, *J. Am. Chem. Soc.*, 1996, **118**, 9326–9332.
17 P. K. Madhu, A. Goldbourt, L. Frydman and S. Vega, *Chem. Phys. Lett.*, 1999, **307**, 41–47.
18 H. Colaux, D. M. Dawson and S. E. Ashbrook, *J. Phys. Chem. A*, 2014, **118**, 6018–6025.
19 A. P. M. Kentgens and R. Verhagen, *Chem. Phys. Lett.*, 1999, **300**, 435–443.
20 T. Vosegaard, P. Florian, D. Massiot and P. J. Grandinetti, *J. Chem. Phys.*, 2001, **114**, 4618–4624.
21 R. Siegel, T. T. Nakashima and R. E. Wasylishen, *Chem. Phys. Lett.*, 2005, **403**, 353–358.
22 Z. Yao, H. T. Kwak, D. Sakellariou, L. Emsley and P. J. Grandinetti, *Chem. Phys. Lett.*, 2000, **327**, 85–90.
23 T. Vosegaard, F. H. Larsen, H. J. Jacobsen, P. D. Ellis and N. C. Nielsen, *J. Am. Chem. Soc.*, 1997, **119**, 9055–9056.
24 Z. Gan and H. T. Kwak, *J. Magn. Reson.*, 2004, **168**, 346–351.
25 J. P. Amoureux, L. Delevoye, S. Steuernagel, Z. Gan, S. Ganapathy and L. Montagne, *J. Magn. Reson.*, 2005, **172**, 268–278.
26 J. P. Amoureux, L. Delevoye, G. Fink, F. Taulelle, A. Flambard and L. Montagne, *J. Magn. Reson.*, 2005, **175**, 285–299.
27 J. P. Amoureux, A. Flambard, L. Delevoye and L. Montagne, *Chem. Commun.*, 2005, 3472–3474.
28 H. T. Kwak and Z. Gan, *J. Magn. Reson.*, 2003, **164**, 369–372.
29 T. J. Ball and S. Wimperis, *J. Magn. Reson.*, 2007, **187**, 343–351.
30 J. W. Wiench, G. Tricot, L. Delevoye, J. Trebosc, J. Frye, L. Montagne, J. P. Amoureux and M. Pruski, *Phys. Chem. Chem. Phys.*, 2006, **8**, 144–150.
31 A. Flambard, L. Montagne, L. Delevoye and S. Steuernagel, *Solid State Nucl. Magn. Reson.*, 2007, **32**, 34–43.
32 Z. Gan, P. L. Gor'kov, W. W. Brey, P. J. Sideris and C. P. Grey, *J. Magn. Reson.*, 2009, **200**, 2–5.
33 R. Hajjar, Y. Millot and P. P. Man, *Prog. Nucl. Magn. Reson. Spectrosc.*, 2010, **57**, 306–342.
34 J. Trebosc, J. P. Amoureux and Z. Gan, *Solid State Nucl. Magn. Reson.*, 2007, **31**, 1–9.
35 M. Bak, J. T. Rasmussen and N. C. Nielsen, *J. Magn. Reson.*, 2000, **147**, 296–330.
36 J. Skibsted, N. C. Nielsen, H. Bildsøe and H. J. Jakobsen, *J. Am. Chem. Soc.*, 1993, **115**, 7351–7362.
37 J. P. Amoureux, M. Pruski, D. P. Lang and C. Fernandez, *J. Magn. Reson.*, 1998, **131**, 170–175.
38 O. B. Lapina, D. F. Khabibulin, K. V. Romanenko, Z. Gan, M. G. Zuev, V. N. Krasil'nikov and V. E. Fedorov, *Solid State Nucl. Magn. Reson.*, 2005, **28**, 204–224.
39 E. Papulovskiy, A. A. Shubin, V. V. Terskikh, C. J. Pickard and O. B. Lapina, *Phys. Chem. Chem. Phys.*, 2013, **15**, 5115–5131.
40 O. B. Lapina, D. F. Khabibulin, A. A. Shubin and V. V. Terskikh, *Prog. Nucl. Magn. Reson. Spectrosc.*, 2008, **53**, 128–191.
41 S. Prasad, P. Zhao, J. Huang, J. J. Fitzgerald and J. S. Shore, *Solid State Nucl. Magn. Reson.*, 2001, **19**, 45–62.
42 D. Massiot, F. Fayon, M. Capron, I. King, S. Le Calvé, B. Alonso, J. O. Durand, B. Bujoli, Z. Gan and G. Hoatson, *Magn. Reson. Chem.*, 2002, **40**, 70–76.
43 D. H. Zhou, G. L. Hoatson and R. L. Vold, *J. Magn. Reson.*, 2004, **167**, 242–252.
44 X. Wang, J. Adhikari and L. J. Smith, *J. Phys. Chem. C*, 2009, **113**, 17548–17559.
45 K. E. Johnston, J. M. Griffin, R. I. Walton, D. M. Dawson, P. Lightfoot and S. E. Ashbrook, *Phys. Chem. Chem. Phys.*, 2011, **13**, 7565–7576.
46 J. V. Hanna, K. J. Pike, T. Charpentier, T. F. Kemp, M. E. Smith, B. E. G. Lucier, R. W. Schurko and L. S. Cahill, *Chem. A Eur. J.*, 2010, **16**, 3222–3239.
47 K. E. Johnston, C. C. Tang, J. E. Parker, K. S. Knight, P. Lightfoot and S. E. Ashbrook, *J. Am. Chem. Soc.*, 2010, **132**, 8732–8746.
48 I. Saouli, S. Landron, B. Peric, A. Boutarfaia, C. Kouvatas, L. Le Pollès, J. Cuny and R. Gautier, *J. Struct. Chem.*, 2019, **60**, 412–419.
49 I. V. Yakovlev, E. Papulovskiy, E. A. Paukshtis, V. M. Bondareva, A. V. Toktarev, V. I. Zaikovskii and O. B. Lapina, *Appl. Magn. Reson.*, 2019, **50**, 589–597.

1 Citations should appear here in the format A. Name, B. Name and C. Name, *Journal Title*, 2000, **35**, 3523; A. Name, B. Name and C. Name, *Journal Title*, 2000, **35**, 3523.
2 …

Formatting – please delete this box prior to submission

- Please be aware, our template aims to give you an idea of what your article will look like, however the final version will be formatted during production and may look different in keeping with our house style.
- Graphics, including tables, will be located at the top or bottom of the column following their first citation in the text during production (unless they are equations, which appear in the flow of the text). They can be single column or double column as appropriate and require appropriate captions.
- Text is not wrapped around any of the graphics.
- During production, sufficient space will be inserted around graphics for clarity of reading; a horizontal bar will also be used to separate all inserted graphics, tables and their captions from the text:

- Please consult the Styles menu for recommended formatting for all text, including footnotes, references, tables, images and captions.

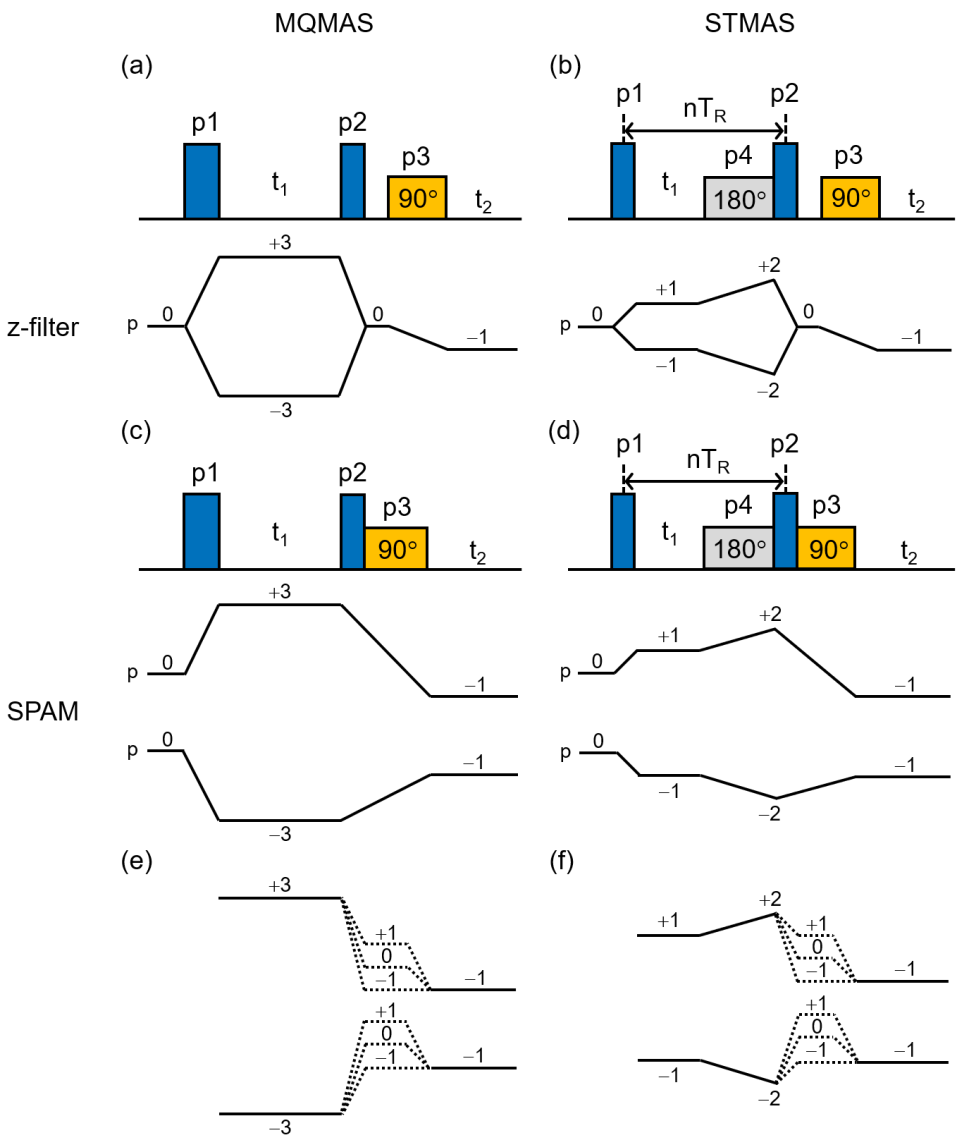

Fig.1. Pulse sequences and coherence transfer pathways of (a) z-filter MQMAS, (b) z-filter STMAS, (c) SPAM-MQMAS and (d) SPAM-STMAS experiments used in the following investigations. The 3QMAS version of MQMAS and the DQF version of STMAS were employed throughout. A conceptual description of available coherence pathways is shown in (e) for SPAM-MQMAS and (f) for SPAM-STMAS.

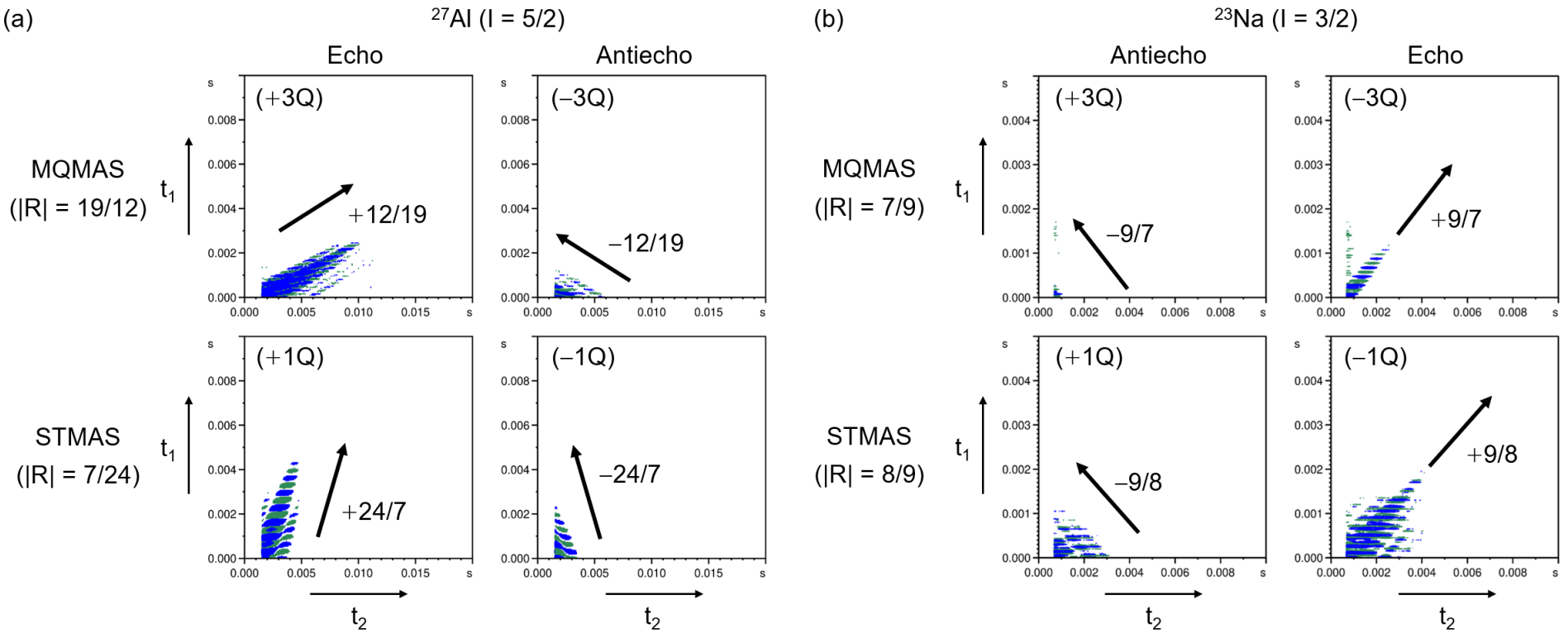

Fig.2. Time-domain representation of echo (E) and antiecho (AE) signals of SPAM-MQMAS and SPAM-STMAS experiments recorded on (a) ^{27}Al (I = 5/2) of berlinite and (b) ^{23}Na (I = 3/2) of Na_2SO_4 at B_0 = 14.1 T, ν_R = 20 kHz. (a) ^{27}Al MQMAS: NS = 12, RD = 3 s, E = AE = 100, T_{exp} = 2 hrs, ^{27}Al STMAS: NS = 16, RD = 3 s, E = AE = 175, T_{exp} = 2.5 hrs. (b) ^{23}Na MQMAS: NS = 12, RD = 3 s, E = AE = 75, T_{exp} = 1.5 hrs, ^{23}Na STMAS: NS = 16, RD = 1.5 s, E = AE = 100, T_{exp} = 1.3 hrs.

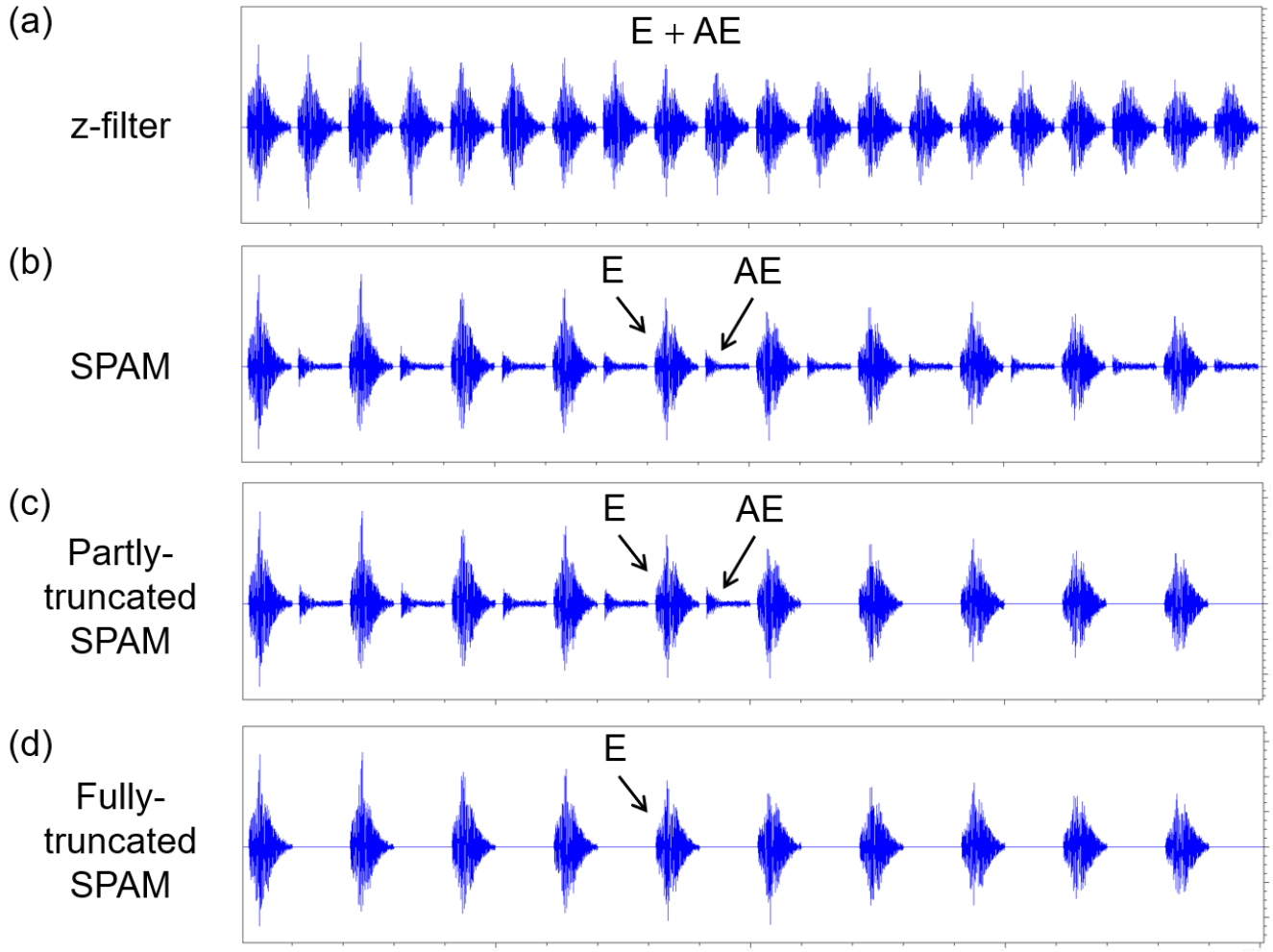

Fig.3. Schematic comparison of a series of 2D FIDs (as found in “FID” tab on TopSpin) for (a) z-filter, (b) SPAM, (c) partly-truncated SPAM and (d) fully-truncated SPAM experiments.

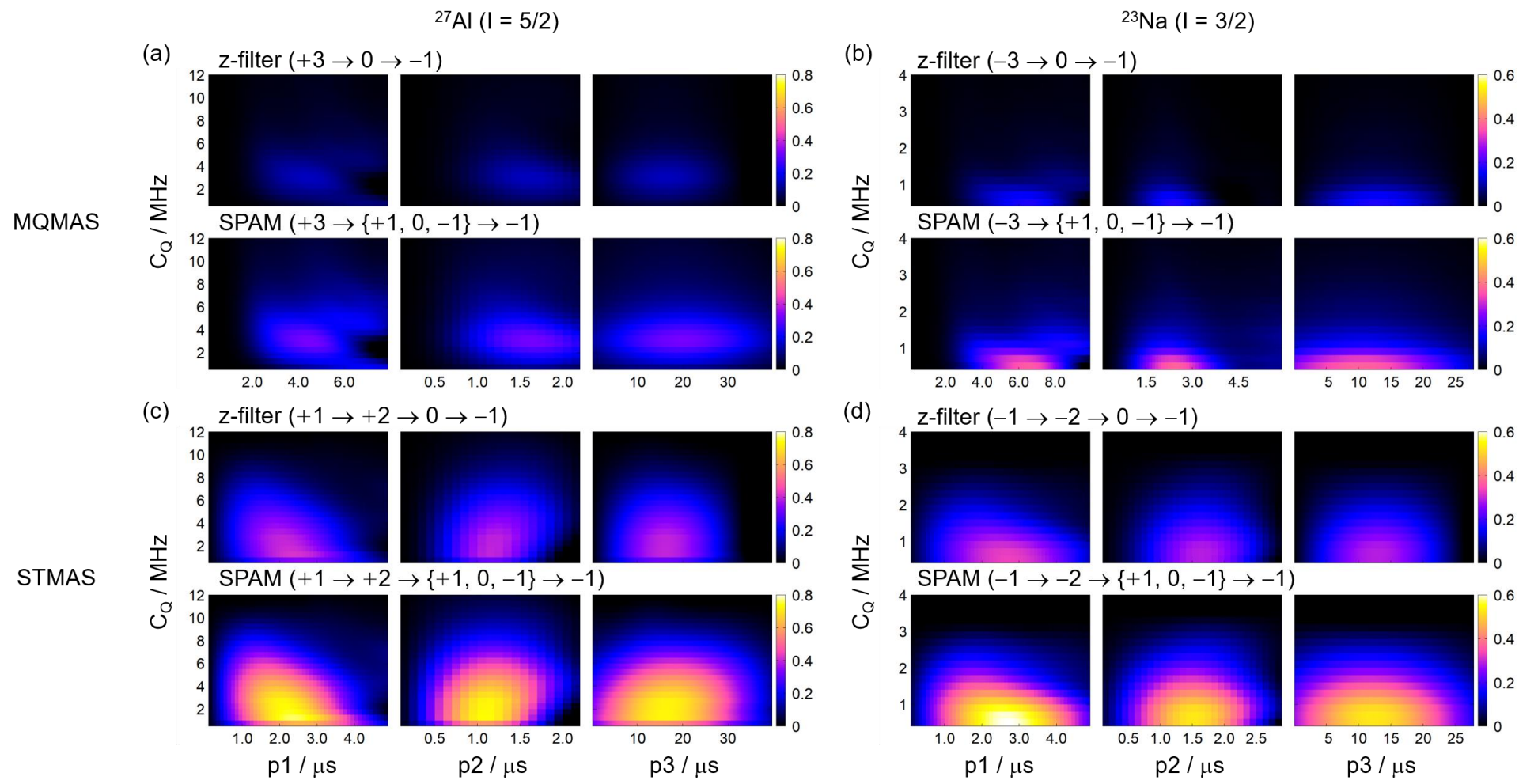

Fig.4. Simulated signal intensity of (a,b) z-filter and SPAM-MQMAS, (c,d) z-filter and SPAM-STMAS with respect to each pulse length (p1, p2, p3) for a range of quadrupolar coupling constants (C_Q) of (a,c) ^{27}Al (I = 5/2) and (b,d) ^{23}Na (I = 3/2) nuclei at B_0 = 14.1 T, ν_R = 20 kHz, $\nu_1(^{27}\text{Al})$: {p1, p2, p3, p4} = {90, 90, 5, 5} kHz, $\nu_1(^{23}\text{Na})$: {p1, p2, p3, p4} = {95, 95, 9.5, 9.5} kHz. Pulse lengths used within each plot: (a) ^{27}Al MQMAS: {p1, p2, p3} = {4.0, 1.4, 16.7} μs, (c) ^{27}Al STMAS: {p1, p2, p3, p4} = {1.8, 1.1, 16.7, 33.3} μs, (b) ^{23}Na MQMAS: {p1, p2, p3} = {6.5, 2.2, 13.0} μs, (d) ^{23}Na STMAS: {p1, p2, p3, p4} = {1.8, 1.6, 13.0, 26.0} μs.

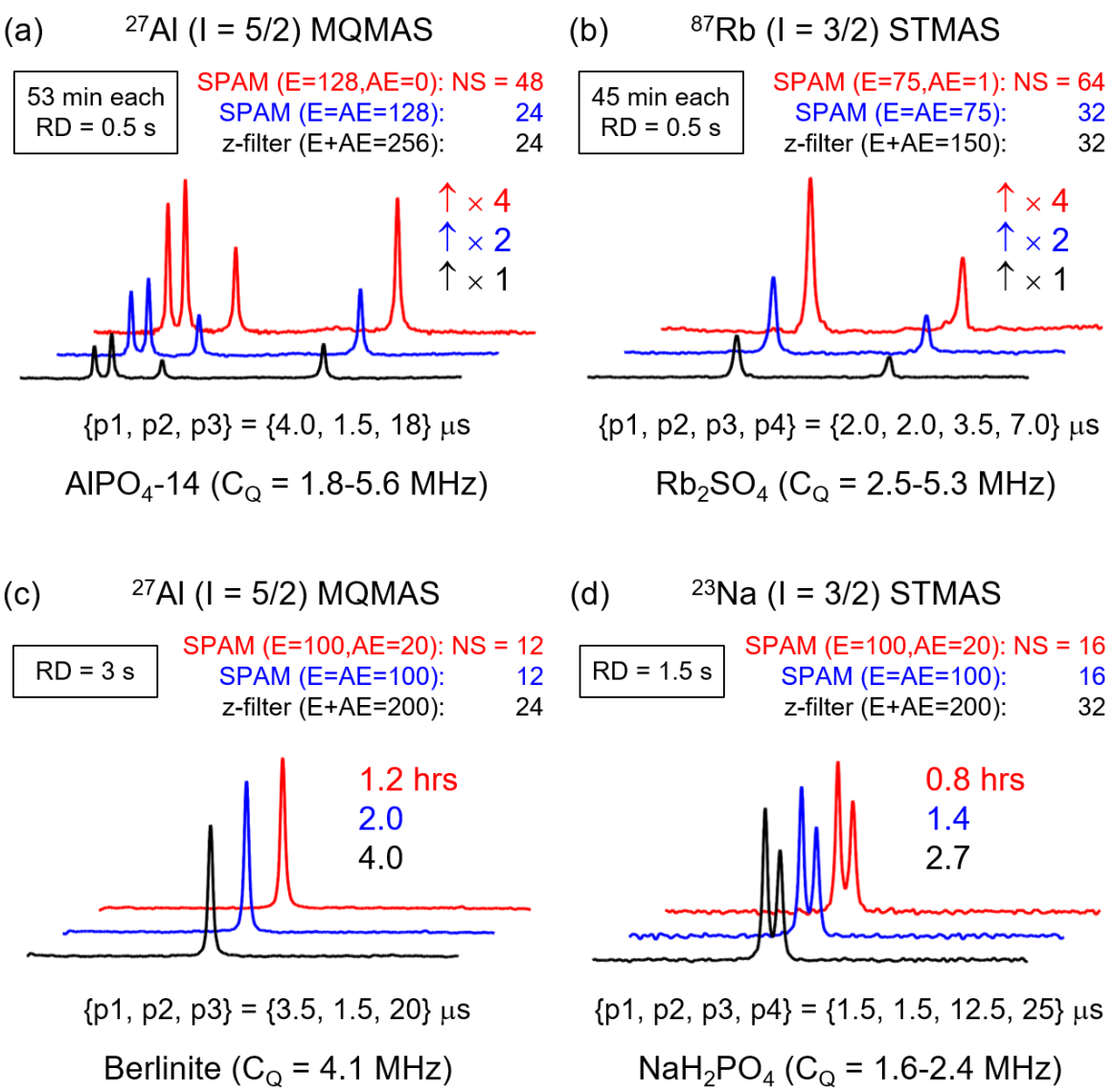

Fig.5. Isotropic projection of MQMAS and STMAS spectra with respect to (a,b) sensitivity enhancement and (c,d) reduction in experimental time using SPAM approaches recorded at B_0 = 14.1 T, ν_R = 20 kHz. $\nu_1(^{27}Al)$: {p1, p2, p3, p4} = {90, 90, 5, 5} kHz, $\nu_1(^{87}Rb)$: {p1, p2, p3, p4} = {120, 120, 45, 45} kHz, $\nu_1(^{23}Na)$: {p1, p2, p3, p4} = {95, 95, 9.5, 9.5} kHz.

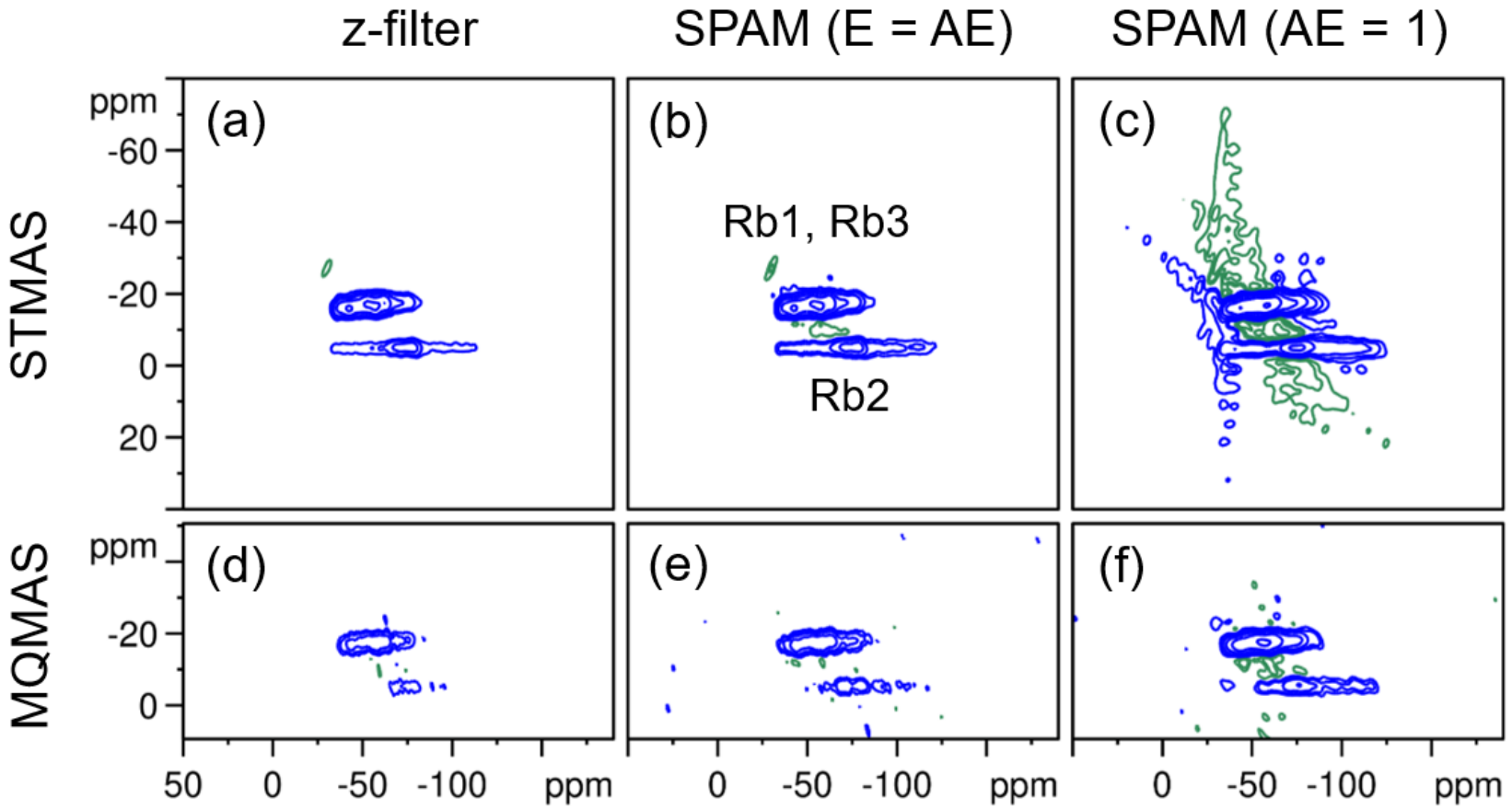

Fig.6. ^{85}Rb (I = 5/2) MQMAS and STMAS spectra of $RbNO_3$ at B_0 = 14.1 T, ν_R = 20 kHz, RD = 0.5 s, T_{exp} = 80 min each, $\nu_1(^{85}Rb)$: {p1, p2, p3, p4} = {35, 35, 9, 9} kHz, MQMAS: {p1, p2, p3} = {8.0, 3.0, 7.5} μs, STMAS: {p1, p2, p3, p4} = {3.0, 3.0, 7.5, 15} μs. (a) E + AE = 100, NS = 96, (b) E = AE = 50, NS = 96, (c) E = 50, AE = 1, NS = 192, (d) E + AE = 50, NS = 192, (e) E = AE = 25, NS = 192, (f) E = 25, AE = 1, NS = 384. P_Q: {Rb1, Rb2, Rb3} = {3.7, 4.9, 3.4} MHz.

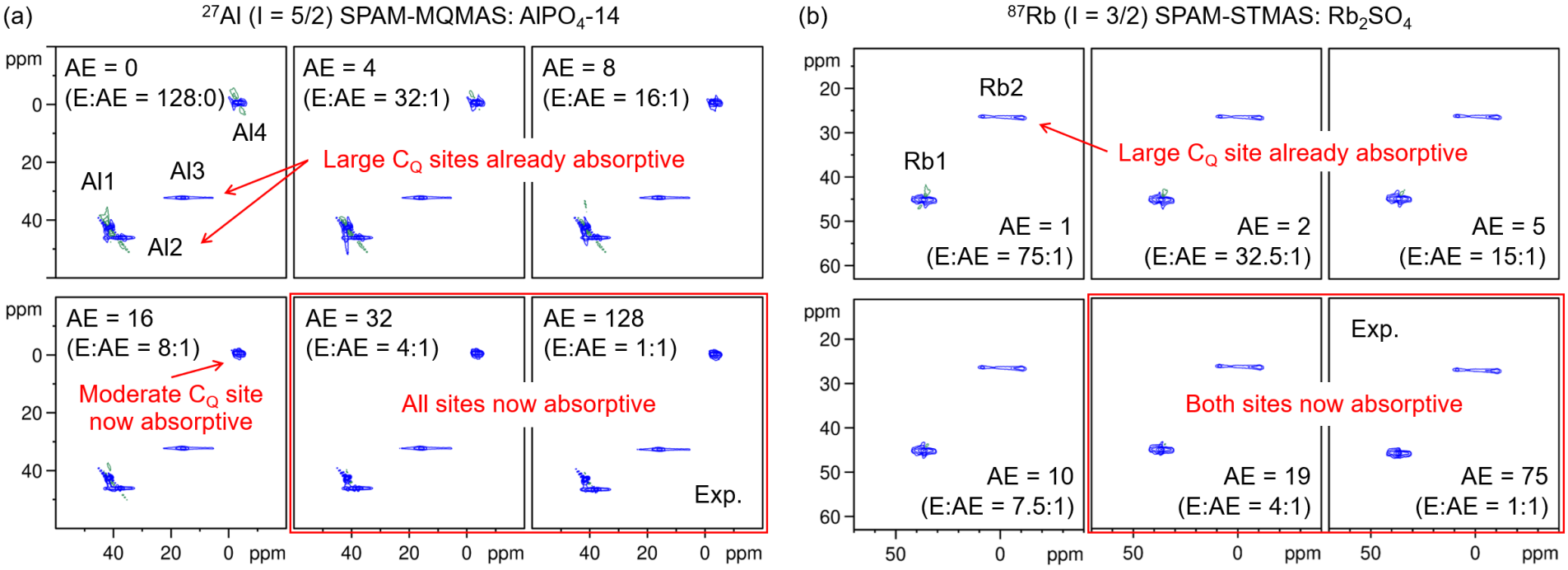

Fig.7. A series of SPAM spectra produced via Fourier Transform of manually zero-filled SPAM datasets. (a) ^{27}Al (I = 5/2) SPAM-MQMAS of AlPO$_4$-14 and (b) ^{87}Rb (I = 3/2) SPAM-STMAS of Rb$_2$SO$_4$ C$_Q$: {Al1, Al2, Al3, Al4} = {1.7, 4.1, 5.6, 2.6} MHz and {Rb1, Rb2} = {2.7, 5.3} MHz.

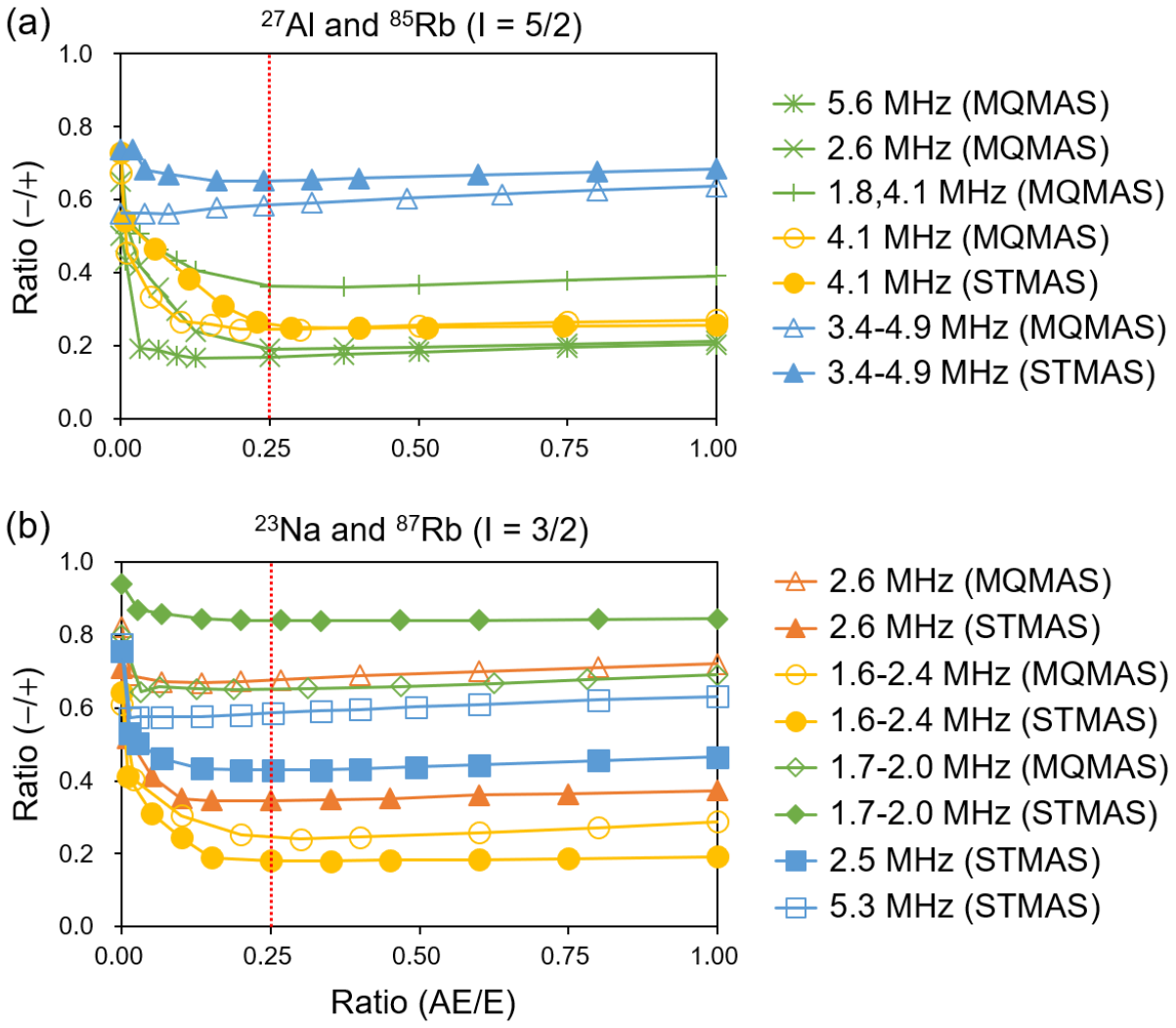

Fig.8. Ratio of negative to positive integral (–/+) versus the ratio of the number of antiecho to echo (AE/E). (a) I = 5/2: $AlPO_4$-14 (green, C_Q = 1.8, 4.1, 5.6, 2.6 MHz), berlinite (yellow, C_Q = 4.1 MHz), $RbNO_3$ (blue, P_Q = 3.4-4.9 MHz). (b) I = 3/2: Na_2SO_4 (orange, C_Q = 2.6 MHz), NaH_2PO_4 (yellow C_Q = 1.6-2.4 MHz), Na citrate (green, P_Q = 1.7-2.0 MHz), Rb_2SO_4 (blue, C_Q = 2.5, 5.3 MHz). An estimated convergence line is indicated at E:AE = 4:1.

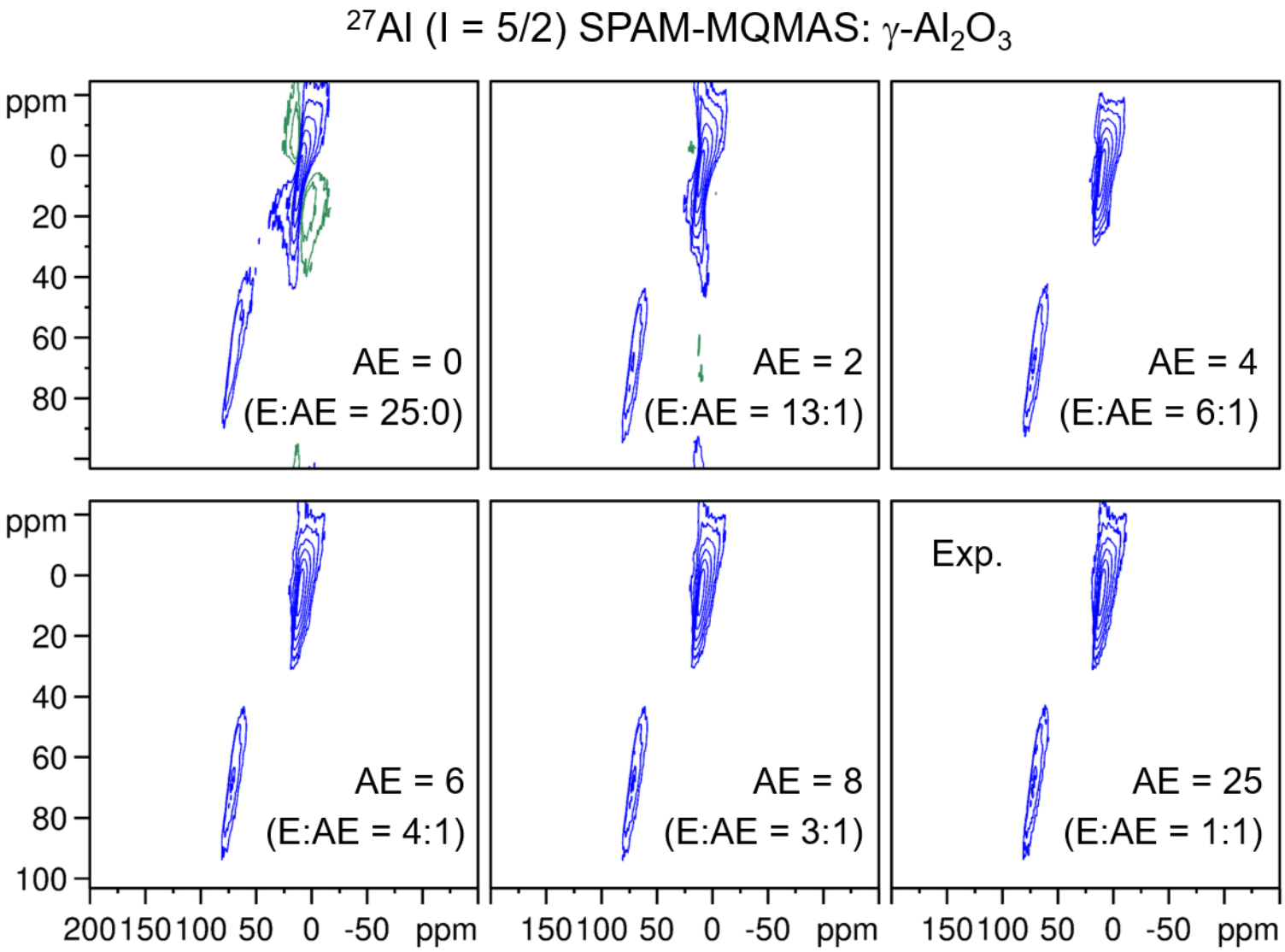

Fig.9. Series of ^{27}Al (I = 5/2) SPAM-MQMAS un-sheared spectra of γ-Al_2O_3 produced via Fourier Transform of manually zero-filled SPAM datasets. B_0 = 14.1 T, ν_R = 20 kHz, NS = 24, RD = 0.5 s, E = 25, T_{exp} = 10 min.

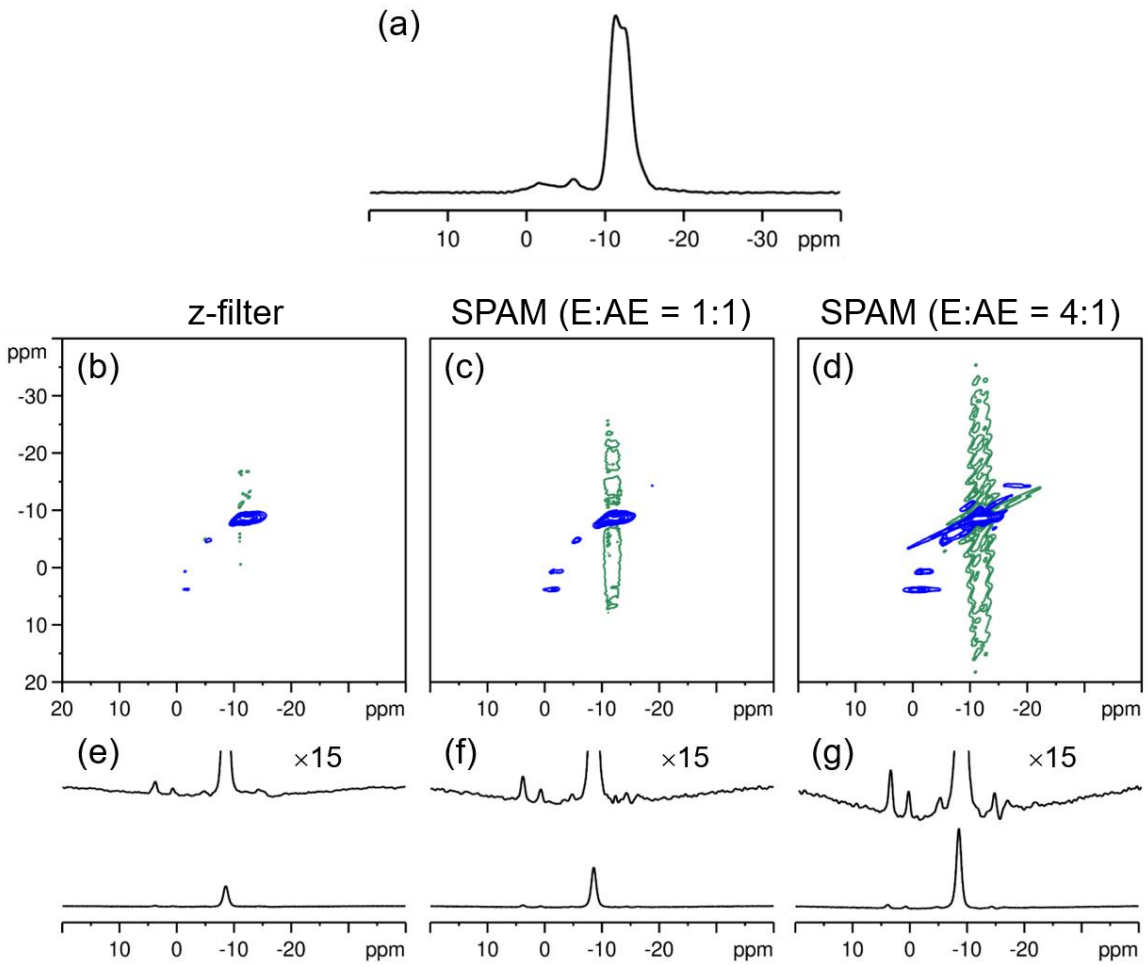

Fig.10. ^{23}Na (I = 3/2) (a) MAS, (b) z-filter STMAS, (c,d) SPAM-STMAS spectra with same contour levels of commercially available $NaVO_3$ at B_0 = 14.1 T, ν_R = 20 kHz and (e-g) corresponding STMAS isotropic projection (bottom) expanded by a factor of 15 (top). $\nu_1(^{23}Na)$: {p1, p2, p3, p4} = {95, 95, 9.5, 9.5} kHz, MAS: p1 = 2.0 μs, STMAS: {p1, p2, p3, p4} = {1.5, 1.5, 15, 30} μs. (a) NS = 1, RD = 30 s, (b) NS = 32, RD = 1 s, E + AE = 192, T_{exp} = 1.7 hrs, (c) NS = 32, RD = 1 s, E = 96, AE = 96, T_{exp} = 1.7 hrs, (d) NS = 64, RD = 1 s, E = 96, AE = 24, T_{exp} = 2.1 hrs.

	z-filter	SPAM (1:1)	SPAM (2:1)	SPAM (4:1)	SPAM (1:0)
Signal (S)	1	≈2	≈2.7	≈3.2	≈4
Noise (N)	1	√2	√2	√2	√2
S/N	1	≈1.4	≈1.9	≈2.3	≈2.8

Table 1. Expected maximum gain over z-filter of signal-to-noise (S/N) ratio of SPAM approaches.

	MQMAS				STMAS			
	z-filter		SPAM (4:1)		z-filter		SPAM (4:1)	
E + AE	96	96			192	192		
E			48	48			96	96
AE			12	12			24	24
RD	0.5	5	0.5	5	0.5	5	0.5	5
NS	720	72	960	96	320	32	480	48
T_{exp}	9h48n	9h37m	8h20m	8h2m	8h44m	8h33m	8h21m	8h2m
S/N (F2)								
Na1	72.55	141.11	165.62	300.47	385.21	604.37	767.94	1054.42
Na2	78.21	76.55	183.91	181.19	450.11	315.53	726.37	580.52
Na3	31.76	47.55	69.03	129.30	248.51	247.16	444.36	455.70

Table 2 Comparison of MQMAS and STMAS experimental approaches for sodium citrate dihydrate recorded with a comparable experimental time ($T_{exp} \approx 9$ hrs) and corresponding signal-to-noise ratio (S/N) of each Na site obtained from F2 slice using the “sino” command on TopSpin.

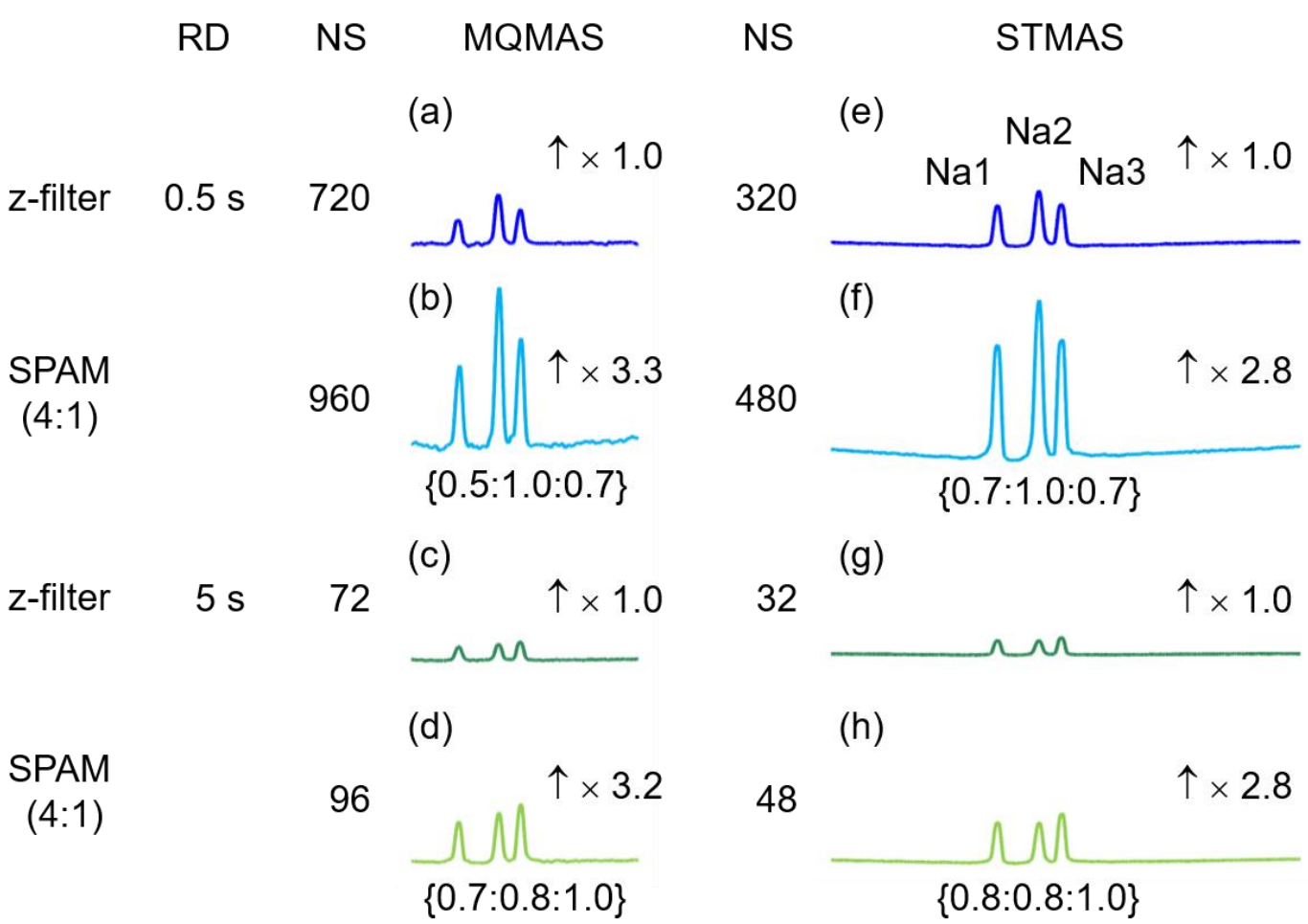

Fig.11. Isotropic projection of ^{23}Na (I = 3/2) MQMAS and STMAS spectra of sodium citrate dihydrate recorded using various experimental approaches (as shown in Table 2) with fixed T_{exp} (8-10 hrs) at B_0 = 14.1 T, ν_R = 20 kHz, $\nu_1(^{23}Na)$: {p1, p2, p3, p4} = {95, 95, 9.5, 9.5} kHz, MQMAS: {p1, p2, p3} = {5.0, 2.5, 15} μs, STMAS: {p1, p2, p3, p4} = {1.5, 1.5, 12.5, 25} μs. P_Q: {Na1, Na2, Na3} = {2.0, 1.9, 1.7} MHz. In (b,d,f,h), the ratios of integrated signal intensities with respect to the highest peak of each spectrum is shown in curly brackets.

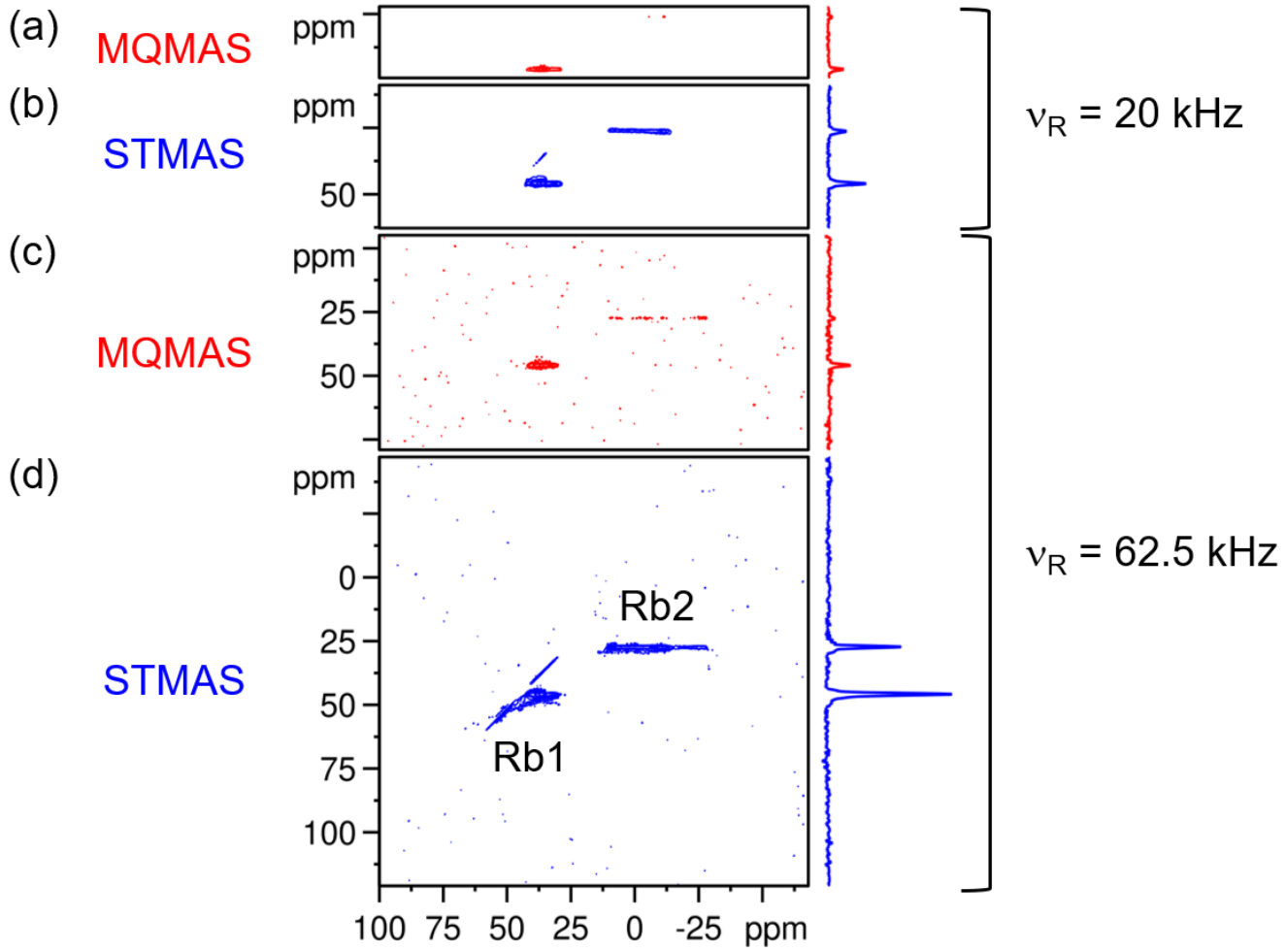

Fig.12. ^{87}Rb (I = 3/2) z-filter (a,c) MQMAS and (b,d) STMAS spectra of Rb_2SO_4 and corresponding isotropic projection at B_0 = 14.1 T, RD = 0.5 s with (a,b) ν_R = 20 kHz or (c,d) ν_R = 62.5 kHz using a 1.3 mm rotor. $\nu_1(^{87}Rb)$: {p1, p2, p3, p4} = {160, 160, 20, 20} kHz, MQMAS: {p1, p2, p3} = {3.0, 1.5, 6} μs, STMAS: {p1, p2, p3, p4} = {1.4, 1.0, 6.0, 10} μs. (a,b) T_{exp} = 0.5 hrs with (a) NS = 72, E + AE = 50, (b) NS = 32, E + AE = 100, (c,d) T_{exp} = 1.5 hrs with (c) NS = 72, E + AE = 160, (d) NS = 32, E + AE = 320. C_Q: {Rb1, Rb2} = {2.5, 5.3} MHz.

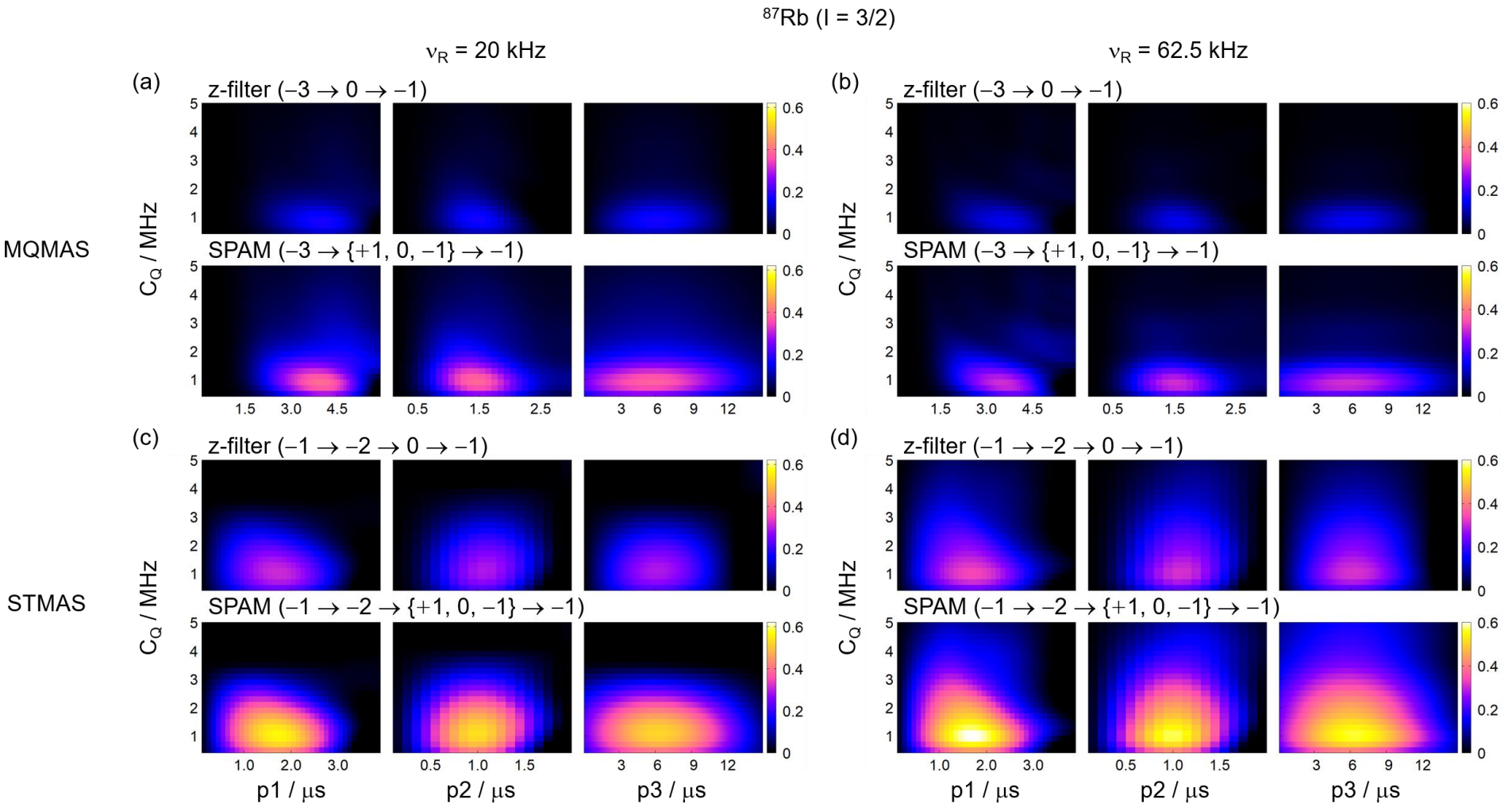

Fig.13. Simulated z-filter and SPAM signal intensity of (a,b) MQMAS and (c,d) STMAS with respect to each pulse length (p1, p2, p3) and C_Q at B_0 = 14.1 T with (a,c) ν_R = 20 kHz or (b,d) ν_R = 62.5 kHz. $\nu_1(^{87}Rb)$: {p1, p2, p3, p4} = {160, 160, 20, 20} kHz. For each plot, the two other pulse lengths were fixed at their optima. Pulse lengths used within each plot: (a,b) {p1, p2, p3} = {3.5, 1.5, 5.0} μs, (c,d) {p1, p2, p3, p4} = {1.2, 1.0, 6.0, 12.0} μs.

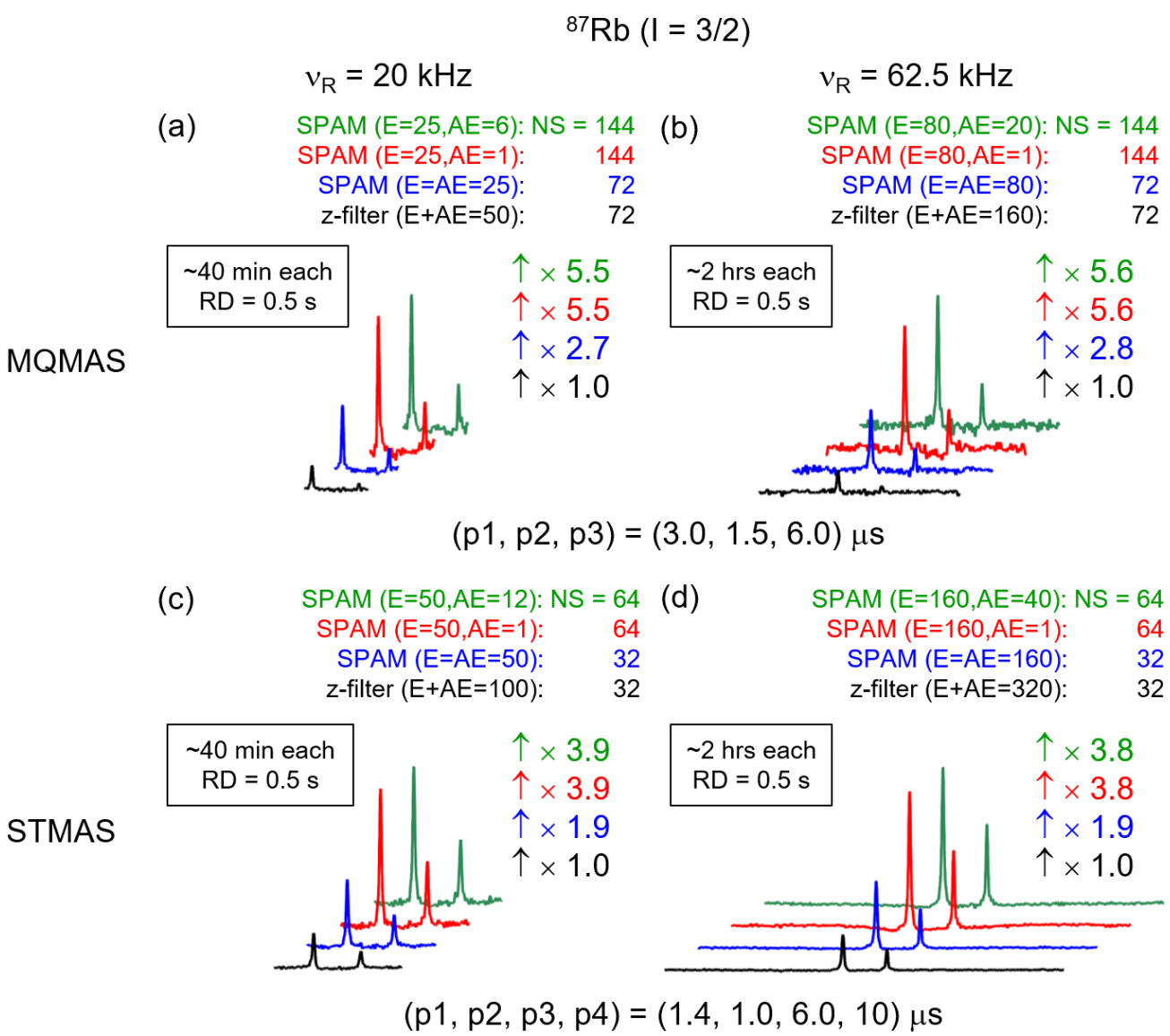

Fig.14. Isotropic projection of ^{87}Rb (I = 3/2) (a,b) MQMAS and (c,d) STMAS spectra of Rb_2SO_4 recorded with various SPAM approaches at B_0 = 14.1 T with (a,c) ν_R = 20 kHz or (b,d) ν_R = 62.5 kHz using a 1.3 mm rotor. $\nu_1(^{87}Rb)$: {p1, p2, p3, p4} = {160, 160, 20, 20} kHz. C_Q: {Rb1, Rb2} = {2.7, 5.3} MHz.

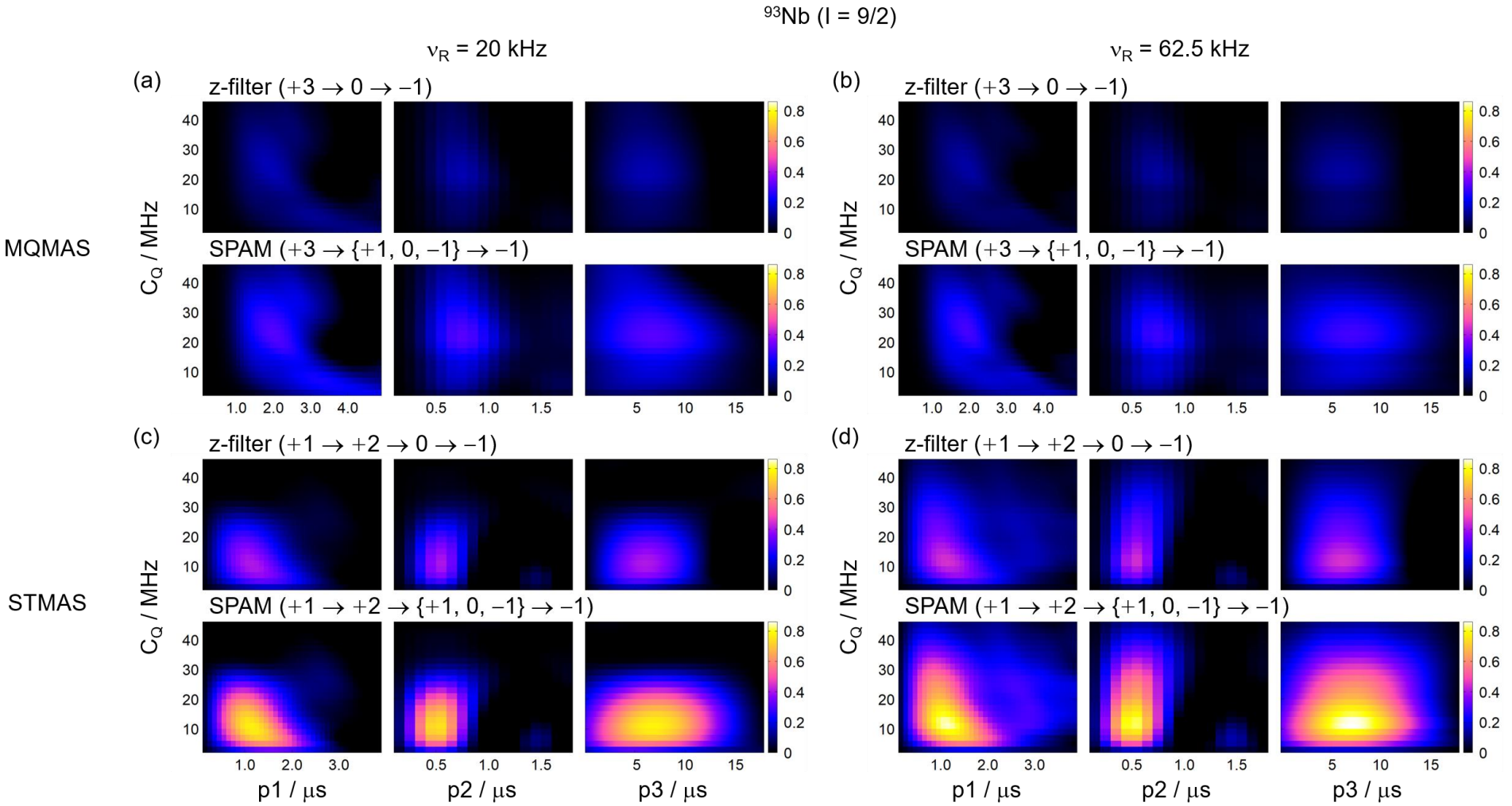

Fig.15. Simulated z-filter and SPAM signal intensity of (a,b) MQMAS and (c,d) STMAS with respect to each pulse length (p1, p2, p3) and C_Q at B_0 = 14.1 T with (a,c) ν_R = 20 kHz or (b,d) ν_R = 62.5 kHz. $\nu_1(^{93}Nb)$: {p1, p2, p3, p4} = {128, 128, 8, 8} kHz. For each plot, the two other pulse lengths were fixed at their optima. Pulse lengths used within each plot: (a,b) {p1, p2, p3} = {2.0, 0.6, 6.0} μs, (c,d) {p1, p2, p3, p4} = {1.0, 0.4, 6.0, 12.0} μs.

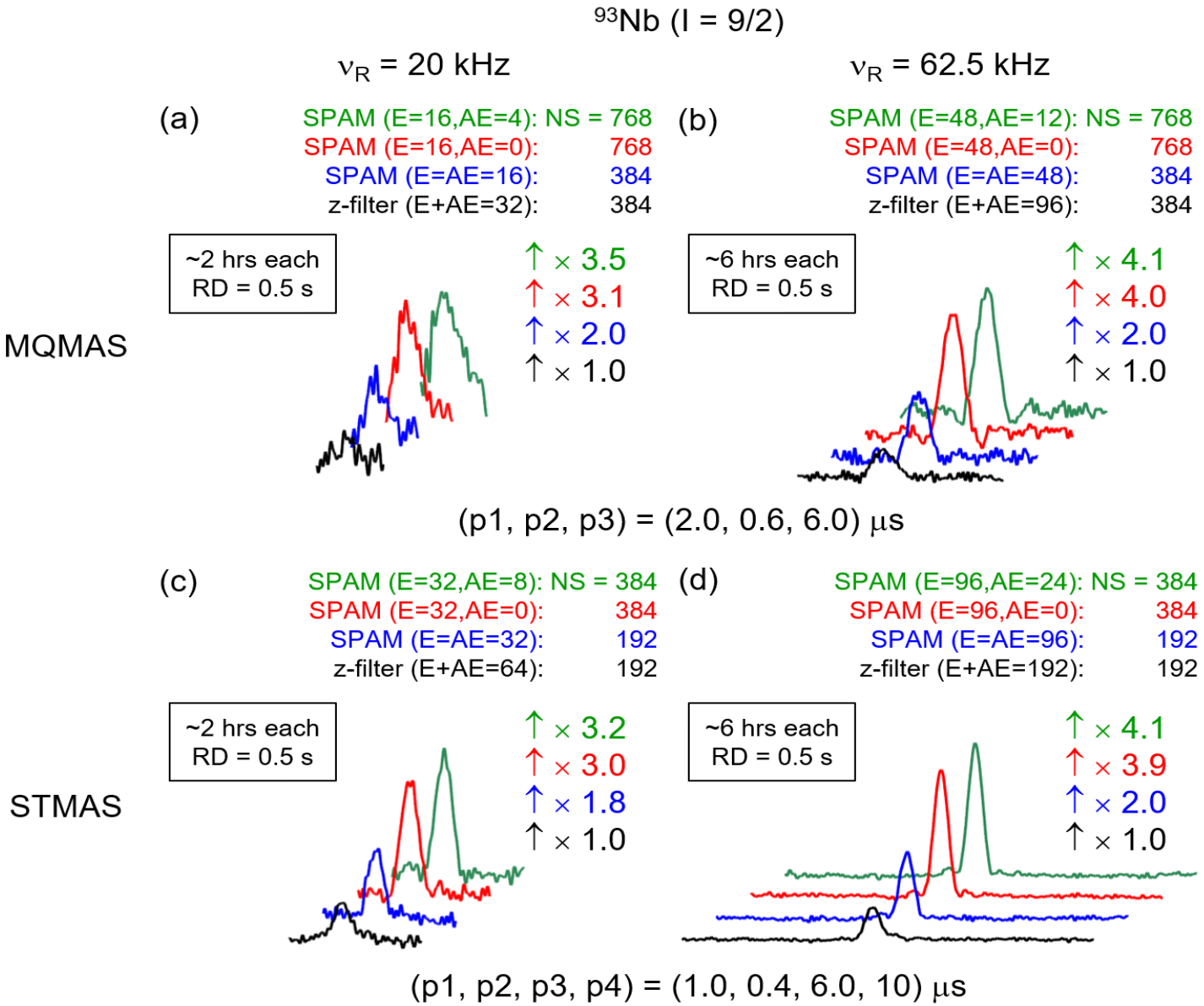

Fig.16. Isotropic slice of ^{93}Nb (I = 9/2) (a,b) MQMAS and (c,d) STMAS spectra of $Nb_3(NbO)_2(PO_4)_7$ recorded with various SPAM approaches at B_0 = 14.1 T with (a,c) ν_R = 20 kHz or (b,d) ν_R = 62.5 kHz using a 1.3 mm rotor. $\nu_1(^{93}Nb)$: {p1, p2, p3, p4} = {128, 128, 8, 8} kHz.

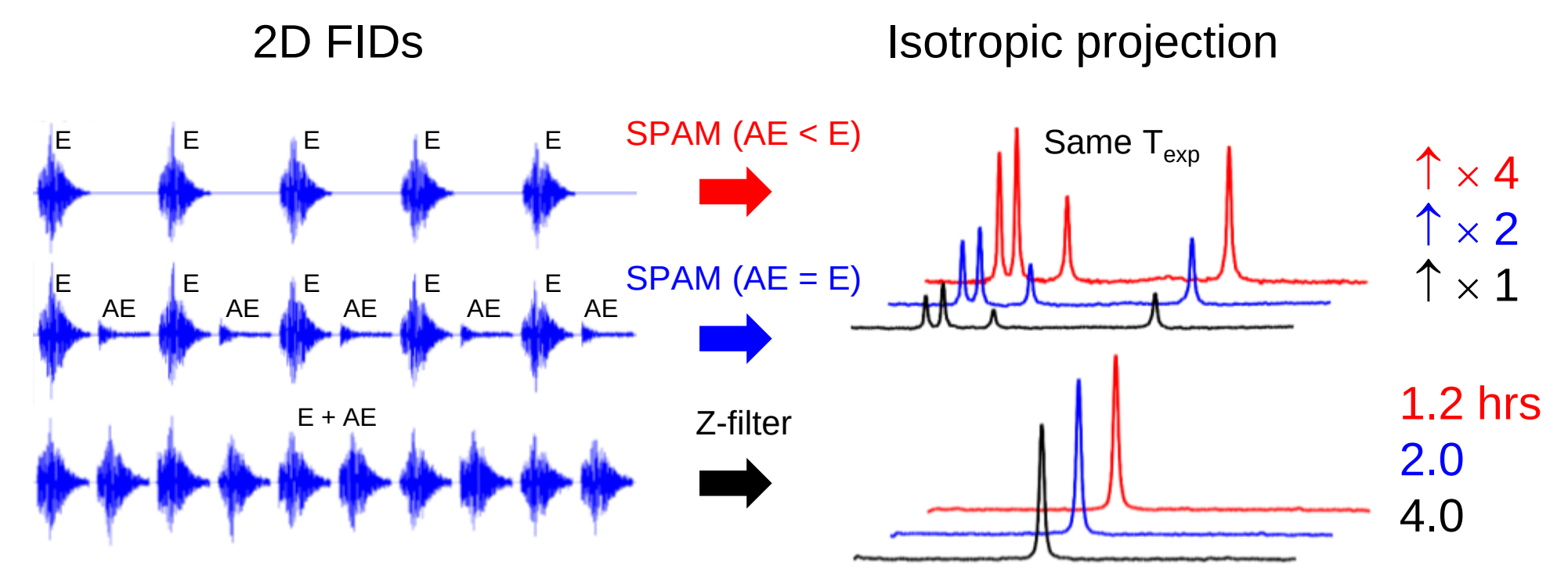
2D FIDs
Isotropic projection
E
E
E
E
E
E
AE
E
AE
E
AE
E
AE
E
AE
E + AE
SPAM (AE < E)
SPAM (AE = E)
Z-filter
Same T exp
× 4
× 2
× 1
1.2 hrs
2.0
4.0